JCB: **Article**

BDNF and its pro-peptide are stored in presynaptic dense core vesicles in brain neurons

Sandra Dieni,[1] Tomoya Matsumoto,[2] Martijn Dekkers,[2] Stefanie Rauskolb,[2] Mihai S. Ionescu,[2] Ruben Deogracias,[2] Eckart D. Gundelfinger,[3] Masami Kojima,[4,5] Sigrun Nestel,[1] Michael Frotscher,[1] and Yves-Alain Barde[2]

[1]Department of Neuroanatomy, Institute of Anatomy and Cell Biology, Albert-Ludwigs-University Freiburg, 79104 Freiburg, Germany
[2]Biozentrum, University of Basel, CH-4056 Basel, Switzerland
[3]Department of Neurochemistry and Molecular Biology, Leibniz Institute for Neurobiology, 39118 Magdeburg, Germany
[4]Biointerface Research Group, Health Research Institute, National Institute of Advanced Industrial Science and Technology, Ikeda 563-8577, Japan
[5]Core Research for Evolutional Science and Technology, Japan Science and Technology Agency, Kawaguchi 332-0012, Japan

THE JOURNAL OF CELL BIOLOGY

Although brain-derived neurotrophic factor (BDNF) regulates numerous and complex biological processes including memory retention, its extremely low levels in the mature central nervous system have greatly complicated attempts to reliably localize it. Using rigorous specificity controls, we found that antibodies reacting either with BDNF or its pro-peptide both stained large dense core vesicles in excitatory presynaptic terminals of the adult mouse hippocampus. Both moieties were ~10-fold more abundant than pro-BDNF. The lack of postsynaptic localization was confirmed in *Bassoon* mutants, a seizure-prone mouse line exhibiting markedly elevated levels of BDNF. These findings challenge previous conclusions based on work with cultured neurons, which suggested activity-dependent dendritic synthesis and release of BDNF. They instead provide an ultrastructural basis for an anterograde mode of action of BDNF, contrasting with the long-established retrograde model derived from experiments with nerve growth factor in the peripheral nervous system.

Introduction

Polarized cells use well-conserved mechanisms to sort proteins into specific compartments (Mellman and Nelson, 2008), providing them with a directionality that is critically important for both their function and meaningful integration into tissues. Central nervous system (CNS) neurons are prototypically polarized cells with specialized axonal and dendritic compartments that play essential roles in intercellular signaling. Although neurons typically communicate by releasing low–molecular weight neurotransmitters accumulated in synaptic vesicles, they also store and release peptides or small

proteins such as brain-derived neurotrophic factor (BDNF), a member of the neurotrophin family. BDNF is known to regulate a wide variety of brain functions in humans, ranging from food intake (Gray et al., 2006) to memory retention (Egan et al., 2003). Indeed, a single amino acid replacement in pro-BDNF has been convincingly shown to correlate with a diminished capacity to remember words and sentences (Egan et al., 2003; Cathomas et al., 2010). Furthermore, in animal models of disease, reduced levels of BDNF have been associated with several conditions, including depression (Calabrese et al., 2007), Rett syndrome (Chang et al., 2006), and Huntington's disease (Zuccato et al., 2010).

Although many aspects of BDNF biology in the adult brain are thus beginning to be well appreciated, the subcellular localization of this secreted protein in neurons of the adult CNS is still very unclear, in large part because of the very low levels of endogenous BDNF. To address this question, several studies have resorted to neuronal cultures prepared from the embryonic

Correspondence to Yves-Alain Barde: yves.barde@unibas.ch

T. Matsumoto's present address is Dept. of Psychiatry and Neurosciences, Division of Frontier Medical, Graduate School of Biomedical Sciences, Hiroshima University, Minami-ku, Hiroshima 734-8551, Japan.

S. Rauskolb's present address is Institute for Clinical Neurobiology, University of Würzburg, 97076 Würzburg, Germany.

M. Frotscher's present address is Center for Molecular Neurobiology Hamburg, D-20251 Hamburg, Germany.

Abbreviations used in this paper: BDNF, brain-derived neurotrophic factor; CCK, cholecystokinin; CNS, central nervous system; DCV, dense core vesicle; DG, dentate gyrus; GFAP, glial fibrillary acidic protein; IP, immunoprecipitation; IR, immunoreactivity; LTP, long-term potentiation; MFB, mossy fiber bouton; PB, phosphate buffer; SL, stratum lucidum; SL-M, stratum lacunosum–moleculare; SR, stratum radiatum; SYP, synaptophysin; WB, Western blotting; WT, wild type.

The Rockefeller University Press $30.00
J. Cell Biol. Vol. 196 No. 6   775–788
www.jcb.org/cgi/doi/10.1083/jcb.201201038

JCB   775

Figure 1. **α-BDNF, α-Myc, and α–pro-BDNF antibodies all generate similar staining patterns.** (A) A schematic representation of the BDNF precursor pro-BDNF and the two cleavage products pro-peptide and BDNF. (B) Low-power view of a WT hippocampal section stained with anti-BDNF antibodies. Note the intense staining in the hilus of the DG and in SL of CA3, each of which contains the axon terminals of mossy fibers. (C and D) Higher magnification view of the DG (C) and CA3 region (D) of the *cbdnf ko* hippocampus stained with anti-BDNF. Note the absence of immunoreactive signals in all cellular and neuropil layers. GCL, granule cell layer; H, hilus; IML, inner molecular layer; PCL, pyramidal cell layer. (E) *Bdnf-Myc* hippocampi stained with Myc antibodies show a similar staining pattern to that produced by BDNF antibodies. (F and G) Note the absence of staining in the corresponding DG (F) and CA3 regions (G) of WT sections treated with Myc antibodies. (H) Polyclonal pro-BDNF antibodies yield a similar pattern to that of anti-BDNF. (I and J) The same antibodies do not produce an immunoreactive signal in hippocampal sections from *cbdnf ko* animals. (B, E, and H) Arrows denote the end bulb of the mossy fiber projection, which delineate CA3 and CA1. Note the relative lack of staining in CA1 in WT and *Bdnf-Myc* sections. Bars: (B, E, and H) 500 µm; (C, F, and I) 100 µm; (D, G, and J) 50 µm.
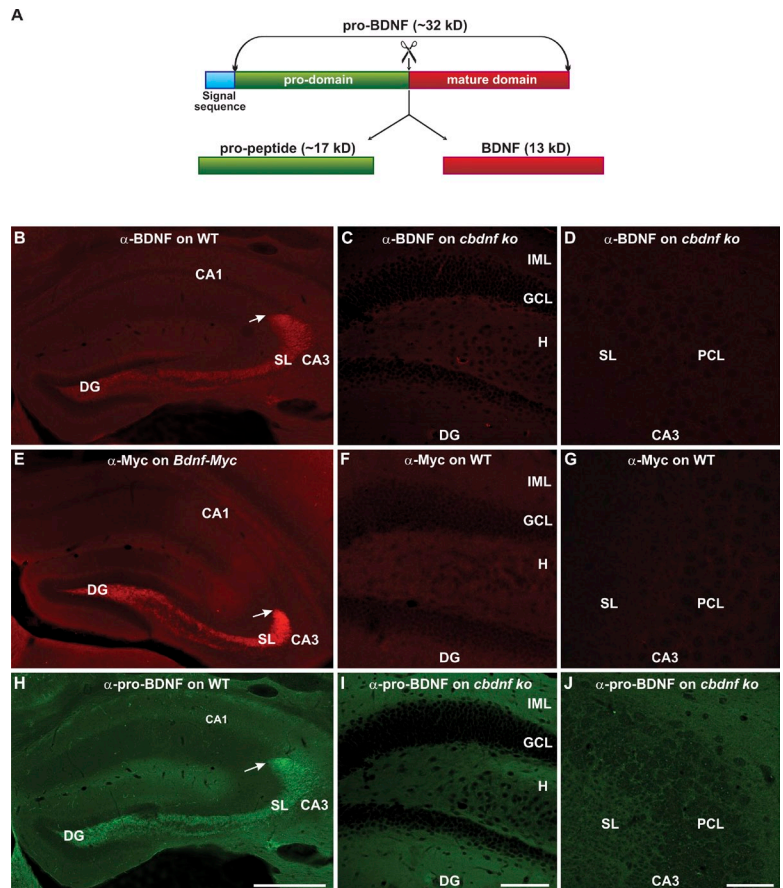
rodent hippocampus (Goodman et al., 1996; Hartmann et al., 2001; Kojima et al., 2001; Egan et al., 2003; Adachi et al., 2005; Dean et al., 2009; Matsuda et al., 2009; Jakawich et al., 2010). In most cases, conclusions about the localization of BDNF were inferred from visualization experiments using transfected tagged BDNF constructs, with recent studies concluding that BDNF is transported in and released from both axons and dendrites (Adachi et al., 2005; Dean et al., 2009; Matsuda et al., 2009; Jakawich et al., 2010). As firmly established by in situ hybridization studies, the *Bdnf* gene is expressed in an activity-dependent fashion by numerous excitatory neurons (Zafra et al., 1990), with protein levels increasing by ∼10-fold during the first 3 wk after birth, in parallel with the development of synaptic activity (Tao et al., 1998; Kolbeck et al., 1999). Nonetheless, BDNF remains, even in the adult brain, an extremely rare protein, making its unambiguous detection in vivo a challenging task that is further complicated by the early death of *Bdnf*-null mutant animals, thus precluding their use as age-matched controls (CONs; Ernfors et al., 1994; Jones et al., 1994).

Given that an understanding of the mode of action of secreted proteins depends on a detailed knowledge of their subcellular localization, the present study investigates the distribution of BDNF in the adult hippocampus at both light microscopic and ultrastructural levels using three lines of transgenic animals: (1) a BDNF knockin line allowing the use of antibodies directed against a tagged version of the BDNF gene (Matsumoto et al., 2008), (2) a line conditionally lacking BDNF in adult neurons allowing for the specificity control of BDNF antibodies

(Rauskolb et al., 2010), and (3) a mutant line displaying seizure episodes that are accompanied by markedly elevated levels of BDNF (Heyden et al., 2011). Antibodies against the BDNF prodomain were also used as an independent means of localizing BDNF as well as to generate information about the status of its cleaved prodomain (described hereon as the pro-peptide).

Results

Antibodies to BDNF and pro-BDNF reveal similar staining patterns

Hippocampal sections prepared from 8-wk-old animals were incubated either with the monoclonal BDNF antibody Mab#9 (anti-BDNF; Fig. 1 B) or with polyclonal antibodies recognizing the BDNF prodomain (anti–pro-BDNF; Fig. 1 H). Tissues from age-matched mice engineered to delete BDNF from neurons (*cbdnf ko*; Rauskolb et al., 2010) were used as a negative CON (Fig. 1, C, D, I, and J). In addition, sections from a knockin mouse line expressing *Bdnf-Myc* (Fig. 1 E; Matsumoto et al., 2008) were incubated with Myc antibodies (anti-Myc), with wild-type (WT) tissue used as a CON (Fig. 1, F and G). These three unrelated antibodies yielded strikingly similar staining patterns (Fig. 1, B, E, and H). In particular, BDNF-, pro-BDNF–, and Myc-immunoreactivity (IR) were each most prominently distributed in the cell bodies and axon terminals of the mossy fiber projection pathway, whereas the layers comprising the CA1 area were only weakly stained, especially in the septal hippocampus.
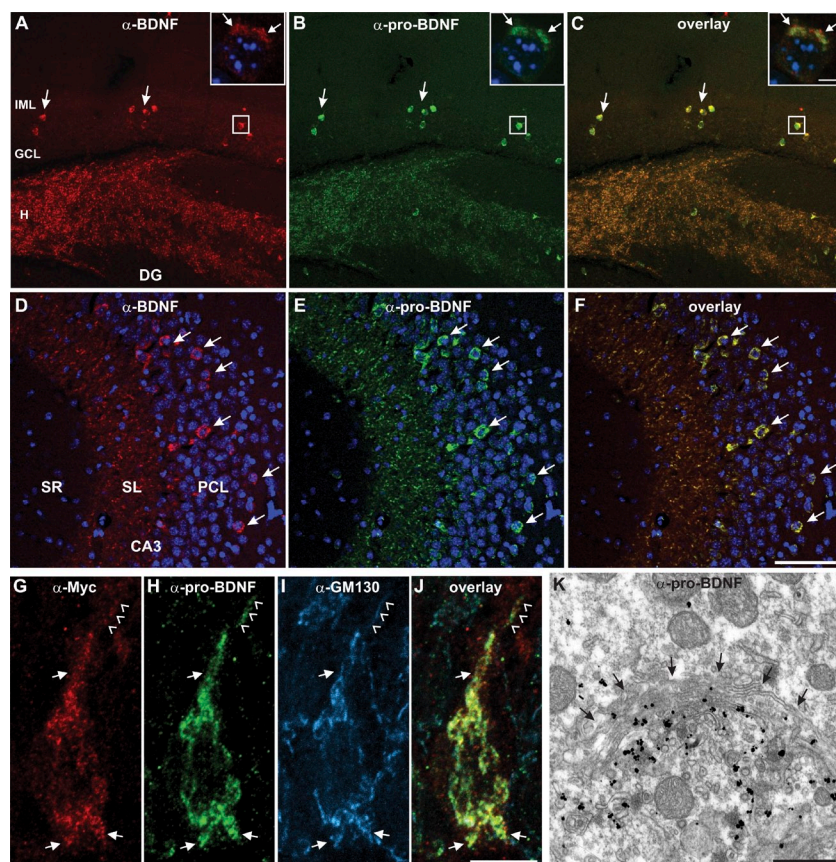
Figure 2. **Detection of BDNF-IR and pro-BDNF–IR in subsets of principal neurons.** (A–C) Low-power confocal stack of the DG. The same subset of granule cells (arrows) coexpresses BDNF-IR (A) and pro-BDNF–IR (B). Boxed areas are enlarged in the inset images showing single BDNF-positive (A) and pro-BDNF–positive (B) granule cells counterstained with DAPI (blue), with labeling concentrated at the cell apex in distinct clusters (arrows) and partial overlap of BDNF and pro-BDNF signals (C, inset). GCL, granule cell layer; H, hilus; IML, inner molecular layer. (C) The merged image reveals an overlap of both signals. (D–F) Confocal stack of area CA3, demonstrating BDNF-IR (D) and pro-BDNF–IR (E) in a subset of pyramidal cell somata (arrows). Nuclei are labeled with DAPI. The prominent band of IR in SL corresponds to the terminal portions of the mossy fiber projection. PCL, pyramidal cell layer. (F) Note the uniform overlap of red and green signals in the overlay image. (G–J) High-resolution confocal stack of a single CA3 neuron labeled with antibodies against Myc (G), pro-BDNF (H), and GM130 (I). Note that the Myc-IR (G) and pro-BDNF–IR (H) extending into the apical dendrite (arrowheads) closely correspond to the Golgi complex (J, merged image). Arrows mark initial dendritic segments originating from the cell body. (K) Electron micrograph showing the Golgi complex (delineated by arrows) of a CA3 neuron labeled by anti–pro-BDNF immunogold. Clusters of gold grains aggregate around the cisterns of the Golgi apparatus. Bars: (A–F) 100 µm; (G–J) 10 µm; (K) 500 nm; (A–C, insets) 5 µm.

BDNF-IR is detected in subsets of neurons

Low-power examination of BDNF-IR in the dentate gyrus (DG) revealed a subset of immunopositive granule cells in the supra- and infrapyramidal blades (Fig. 2 A). BDNF-IR varied in intensity among the labeled cells, with staining concentrated in the somal apex (Fig. 2 A, inset). Anti–pro-BDNF staining was confined to exactly the same subset of granule cells containing BDNF-IR (Fig. 2, B and C), with somal pro-BDNF–IR also concentrated at the apex (Fig. 2 B, inset). In addition, the hilar region, which contains mossy fiber collateral axons of the granule cells, was intensely stained (Fig. 2, A–C). In the CA3 region, a subset of pyramidal neurons also showed both BDNF-IR (Fig. 2, D and F) and pro-BDNF–IR (Fig. 2, E and F). High-resolution examination of sections labeled with anti-Myc and anti–pro-BDNF, along with antibodies against the Golgi matrix protein GM130, revealed Myc-IR throughout the soma and the initial dendritic segments (Fig. 2 G), whereas pro-BDNF–IR showed a similar, albeit more punctate, distribution (Fig. 2 H). Comparison with GM130-IR showed pro-BDNF–positive puncta closely associated with the Golgi apparatus (Fig. 2, I and J). In line with this, anti–pro-BDNF immunogold labeling localized the protein to the Golgi complex of CA3 somata (Fig. 2 K). In CA1, BDNF and pro-BDNF costaining was also detected in a small number of pyramidal neurons in temporal hippocampus sections (unpublished data).

BDNF-IR and pro-BDNF–IR are both detected in presynaptic terminals

The granule cells give rise to mossy fiber axons, whose targets include the complex spines on proximal dendrites of CA3 neurons. Mossy fibers project through and terminate in stratum lucidum (SL) and are characterized by prominent specialized endings known as mossy fiber boutons (MFBs). Accordingly, strong BDNF-IR and pro-BDNF–IR were observed within SL (Figs. 1 [B, E, and H] and 2 [D–F]). Using high-resolution confocal microscopy, both BDNF-IR and pro-BDNF–IR were found to be colocalized to the same subset of MFBs (Fig. 3, A–C).

Additional markers were then applied to identify the type of vesicles containing BDNF-IR and to compare the distribution of BDNF with other peptides known to be anterogradely transported by granule cells. As expected, BDNF-IR did not colocalize with the synaptic vesicle markers synaptophysin (SYP; Fig. 3, D and E) or VGLUT-1 (Fig. 3, F and G). We then tested possible colocalization with Met-enkephalin (Met-enk), an opioid peptide also derived from a larger precursor protein and stored in dense core vesicles (DCVs; Cheng et al., 1995). In a small proportion of granule cells and their axons, Met-enk–IR was detected throughout the soma and initial dendritic segment (Fig. 3 I). Although Met-enk–positive granule cells invariably coexpressed BDNF-IR (Fig. 3 H), the immunoreactive signals of these two precursor-derived molecules remained separate, suggesting that they do not reside together in the same secretory vesicles (Fig. 3, J and K–M). Similar conclusions were reached with cholecystokinin (CCK), a neuropeptide transported along the mossy fiber projection pathway of the ventral mouse hippocampus (Gall et al., 1986). Double labeling with anti-CCK and -BDNF revealed complete segregation of the two peptides within MFBs (Fig. 3, N–P).

Figure 3. Presynaptic localization of BDNF-IR. (A–C) High-resolution optical slice of SL showing Myc-IR (A) and pro-BDNF–IR (B) in the same subset of MFBs (arrows). (C) Note the significant colocalization of red and green puncta in the overlay. (D and F) Merged images of SL labeled with antibodies to Myc and SYP (D) or Myc and VGLUT-1 (F). (E and G) Although BDNF-positive puncta are closely associated with SYP- and VGLUT-1–positive puncta, closer inspection at high magnification reveals segregation of the two markers (arrows), confirming that BDNF is presynaptically expressed but not in synaptic vesicles. (H–M) Costaining with antibodies against Myc and Met-enk. In the small subset of granule cells that coexpresses Myc-IR (H) and Met-enk–IR (I), puncta are similarly distributed throughout the cell but show little overlap (J). Asterisks mark the positions of the nucleus. Similarly, a small proportion of MFBs (arrows) in SL coexpresses Myc-IR (K) and Met-enk–IR (L); however, in the merged image (M), Myc- and Met-enk–IR puncta do not overlap. (N–P) High-resolution optical slice of SL demonstrating expression of Myc-IR (N) and CCK-IR (O) in mossy fiber terminals. Single asterisks label the CCK-IR profile, and double asterisks label the Myc-IR profile. (P) The merged image indicates complete segregation of the two peptides in the mossy fiber projection. (Q) High-resolution confocal image of SR in the CA1 region of a *BDNF-Myc* mouse. Labeling with anti-Myc antibodies reveals localization of BDNF in fine axonal processes (thin arrows in Q–S). (R) Colabeling with antibodies against synpo reveal the relative location of dendritic spines. (S) An overlay of anti-Myc and anti-synpo–labeled section shows presynaptic localization of BDNF, with close apposition between BDNF-IR and synpo-positive spines (white circles and filled arrows in Q–S). Bars: (A–C, E, G, and K–S) 5 µm; (D) 30 µm; (F) 50 µm; (H–J) 10 µm.
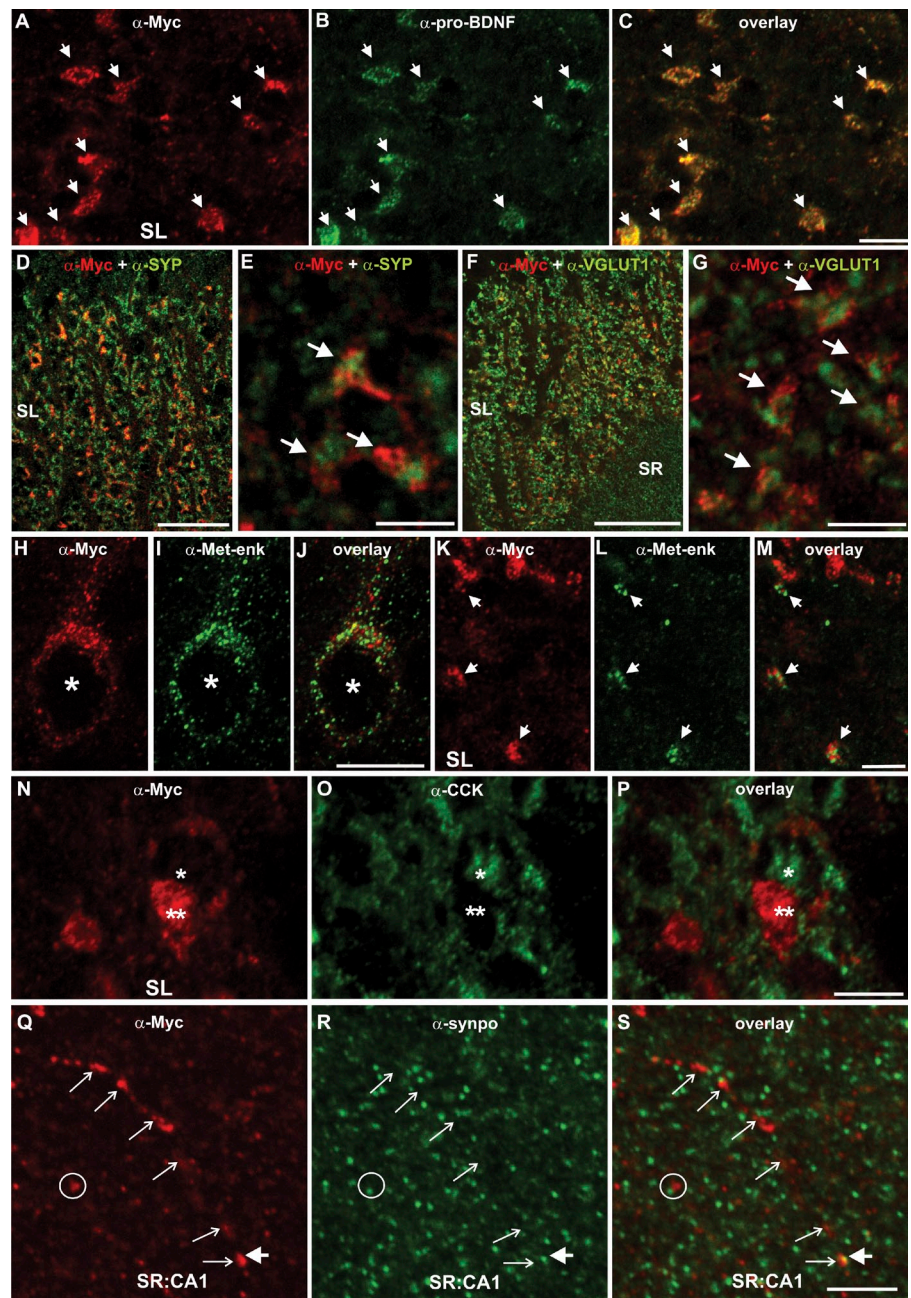
Presynaptic BDNF labeling was also observed in the CA1 region, whereby in stratum radiatum (SR), thin varicose processes labeled with anti-BDNF (Fig. 3, Q–S) and anti–pro-BDNF (not depicted) were sparsely distributed throughout the neuropil, likely corresponding to presynaptic Schaffer collateral axons originating from BDNF-positive CA3 neurons. Importantly, BDNF-IR did not colocalize with the postsynaptic marker synaptopodin (synpo; Fig. 3, R and S).

BDNF and pro-BDNF antibodies label secretory vesicles in presynaptic terminals

Ultrathin sections of SL were then examined at 2,000-fold magnification after immunogold labeling with BDNF and pro-BDNF antibodies. MFBs were identified based on their typical morphological characteristics, namely a high density of synaptic vesicles, numerous synaptic contacts with CA3 complex spines, nonsynaptic *puncta adherentia* at dendritic shafts, and a relatively large surface area. A subset of MFB profiles labeled with anti-BDNF (Fig. 4 A), anti-Myc (not depicted), or anti–pro-BDNF (Fig. 4 B) contained distinct aggregates of gold grains; at 10,000-fold magnification, these gold clusters were found to be associated with large vesicles encompassed by an electron-dense membrane. Although the vesicles were sometimes masked by gold grains, fortuitous grain distribution occasionally revealed an electron-dense core (Fig. 4, A and B, insets). Within MFB profiles of *cbdnf ko* sections, gold grains were never specifically associated with any type of organelle (Fig. 4, C and D). To assess the density of immunogold particles in MFB profiles, gold clusters and single gold grains were quantified in anti-BDNF and anti–pro-BDNF–labeled tissues

and compared between sections from pooled WT/*Bdnf-Myc* mice and *cbdnf ko* mice. Anti-BDNF–labeled MFB profiles showed a mean density of 2.67 ± 0.35 clusters/μm^2 in WT/*Bdnf-Myc* animals compared with 0.38 ± 0.12 clusters/μm^2 (P < 0.005) in *cbdnf ko* profiles (Fig. 4 E). Moreover, single gold grain densities were significantly reduced in *cbdnf ko* MFB profiles, with 5.63 ± 0.94 grains/μm^2 compared with 21.99 ± 2.57 grains/μm^2 in WT/*Bdnf-Myc* (P < 0.005; Fig. 4 F). Similarly, pro-BDNF immunogold labeling showed a mean density of 2.01 ± 0.43 clusters/μm^2 and 27.44 ± 8.21 single grains/μm^2 in MFB profiles from WT/*Bdnf-Myc* animals, whereas in comparison, MFB profiles from *cbdnf ko* animals showed significant reductions in cluster (0.14 ± 0.10/μm^2; P < 0.05; Fig. 4 E) and single grain (5.82 ± 2.06/μm^2; P < 0.05; Fig. 4 F) densities, respectively.

Although BDNF immunogold labeling was mostly concentrated in presynaptic terminals, labeled vesicles were also occasionally observed within unmyelinated axon segments in SL (Fig. 5 A), which in fortuitous sections could be seen to give rise to giant MFBs (Fig. 5 B).

Ultrathin sections of SR (CA1) labeled with anti-BDNF and anti–pro-BDNF immunogold were also examined, and, as expected, large cluster-labeled secretory vesicles were observed within small axon terminals (Fig. 5 C). Depending on the proximal distal level of SR, these infrequent labeled boutons likely correspond to Schaffer collateral terminals or entorhinal terminals. No such labeled terminals were observed in *cbdnf ko* sections (Fig. 5 D).

BDNF-IR and pro–BDNF-IR are not detected in dendrites

Next, we examined the possible localization of BDNF in dendrites by analyzing sections double labeled with anti-Myc and anti–microtubule-associated protein–2 (MAP-2). Both in BDNF-positive granule cells and CA3 neurons, Myc-IR only extended as far as the initial dendritic segments, and there was no evidence of colocalization in SL (Fig. 6, A–C). Sections were alternatively labeled with antibodies to Arc/Arg3.1, an immediate early gene product up-regulated in somata and dendrites during elevated synaptic activity (Lyford et al., 1995). Confocal scanning revealed that the majority of granule cells labeled with BDNF-IR and pro-BDNF–IR also expressed Arc/Arg3.1-IR (Fig. 6, D–G). Although Arc/Arg3.1-IR was seen throughout the soma and dendritic arbor, strong coexpression of BDNF-IR and pro-BDNF–IR was confined to the cell soma (Fig. 6, D–G).

In ultrathin sections prelabeled either with anti-BDNF or anti–pro-BDNF immunogold, gold grains were sparsely distributed within dendritic profiles (Fig. 6, H and K). When profiles were thoroughly scrutinized for specifically labeled vesicles or endosomes, none was found to be stained above the background levels observed in dendrites from *cbdnf ko* sections (Fig. 6, I and L). Gold grain quantification of anti-BDNF–labeled sections (Fig. 6 J) revealed a mean density of 3.56 ± 0.45 grains/μm^2 in WT/*Bdnf-Myc* mice versus 4.72 ± 0.91 grains/μm^2 in *cbdnf ko* mice (P = 0.81). Similarly, in anti–pro-BDNF–stained sections, mean densities were

E   Gold cluster density in MFBs
F   Gold grain density in MFBs
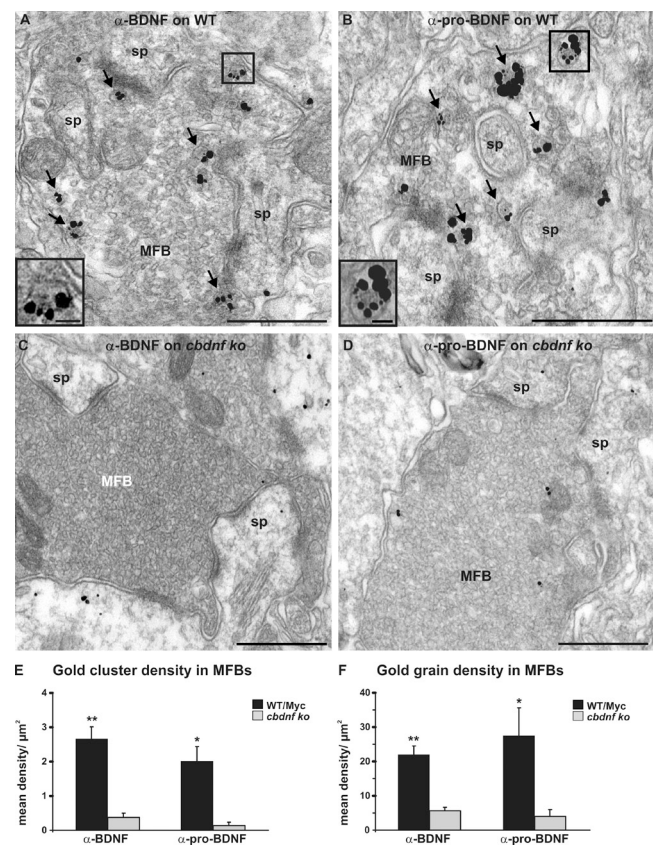
Figure 4.   **Ultrastructural localization of BDNF and pro-BDNF immunogold labeling in MFBs.** (A) Electron micrograph of an ultrathin section of WT SL prelabeled with anti-BDNF immunogold. Numerous gold clusters (arrows) are associated with large secretory vesicles within the bouton (see inset). sp, dendritic spine. (B–D) An anti–pro-BDNF–labeled WT MFB containing cluster-labeled secretory vesicles (arrows). The inset image exemplifies a labeled large DCV. Large secretory vesicles labeled with gold clusters were not found in anti-BDNF–labeled (C) or anti–pro-BDNF–labeled (D) MFBs from *cbdnf ko* mice, confirming the specificity of the signal in WT sections. (E and F) Quantification of BDNF and pro-BDNF immunogold labeling in WT versus *cbdnf ko* MFBs. MFBs from WT and *BDNF-Myc* mice (n = 5 for anti-BDNF and n = 4 for anti–pro-BDNF) have a significantly higher density of gold clusters (E) and single gold grains (F) than MFBs from *cbdnf ko* mice (n = 3). *, P < 0.05; **, P < 0.005. Error bars represent SEM. Bars: (A–D) 500 nm; (A and B, insets) 50 nm.

comparable between WT/*Bdnf-Myc* mice (4.69 ± 1.09 grains/μm^2) and *cbdnf ko* mice (4.08 ± 2.02 grains/μm^2; P = 0.31; Fig. 6 M).

Localization of BDNF-IR and pro-BDNF–IR in *Bsn* mutants

Next, we examined the hippocampus of mice lacking the presynaptic protein Bassoon, as these mutants develop episodic generalized seizures (Altrock et al., 2003) and have enlarged cortices and hippocampi (Angenstein et al., 2007). Concurrent with the development of seizures, BDNF protein levels become significantly higher than those measured in adult CON littermates (see Fig. 10 C; Heyden et al., 2011). Whereas Bassoon (*Bsn*) mutants showed the typical distribution pattern of BDNF-IR and pro-BDNF–IR, a dramatic increase in staining intensity largely confined to the neuropil was observed (compare CON in Fig. 7 [A–D] with *Bsn* in Fig. 7 [E–H]). In contrast, granule cell

Figure 5. **BDNF and pro-BDNF immunogold labeling in preterminal axons.** (A) In sections treated with anti-BDNF antibodies, labeled vesicles (arrows and inset) were observed in unmyelinated mossy fiber axons. (B) An electron micrograph showing a mossy fiber terminating into a bouton (dashed outline). The arrow points to an anti–pro-BDNF–labeled vesicle (see inset), which is likely en route to the terminal. ax, axon; sp, dendritic spine. (C) Anti-BDNF labeling of a presynaptic terminal in SR in CA1. Large silver-enhanced gold clusters (arrows) were observed. at, axon terminal. (D) Anti-BDNF staining of sections from *cbdnf ko* yielded nonspecific background labeling. Bars: (A–D) 500 nm; (A and B, insets) 100 nm.
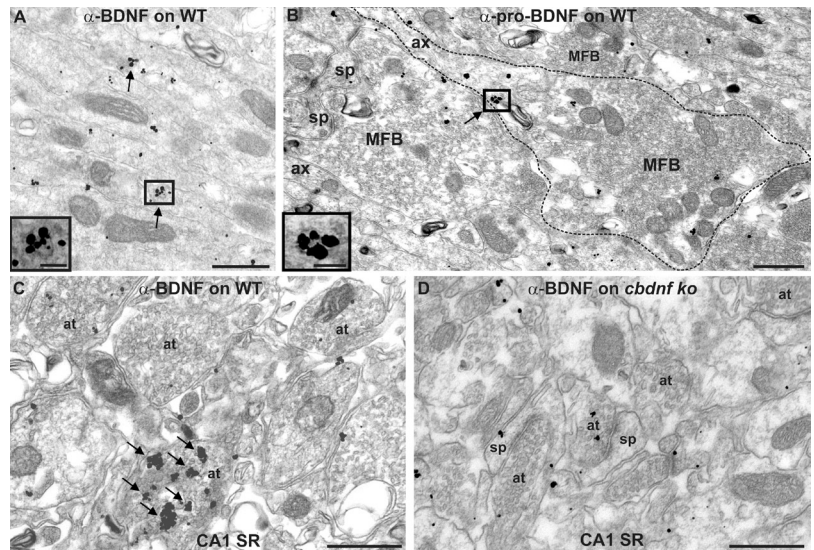
bodies from *Bsn* mutants did not show increases in anti-BDNF (Fig. 7 I) or anti–pro-BDNF (Fig. 7 J) staining intensities, although a much higher proportion of cells was labeled in comparison with CON tissues. Granule cell dendrites in the molecular layer remained unlabeled in *Bsn* mutants, whereas in the CA3 region, the stark increase in BDNF-IR (Fig. 7 G) and pro-BDNF–IR (Fig. 7 H) was confined to SL. Closer examination revealed intense presynaptic labeling in MFB profiles (Fig. 7, K and L), which was confirmed by a lack of colocalization with the postsynaptic markers synpo (Fig. 7 K) and MAP-2 (Fig. 7 L), respectively.

Enhanced BDNF staining in *Bsn* mutants was not only confined to the granule cell–CA3 projection pathway. In the CA1 region, where BDNF-IR can usually only be detected at high magnification (compare Fig. 1 with Figs. 3 Q and 5 D), a conspicuous band of punctate BDNF-IR and pro-BDNF–IR was observed at the border of SR and stratum lacunosum–moleculare (SL-M; Fig. S1, A–C), corresponding to a region known to harbor fibers from the entorhinal cortex (Amaral and Lavanex, 2006). Importantly, these increased signals colocalized (Fig. S1 D), showing no overlap with either synpo-IR (Fig. S1 E) or glial fibrillary acidic protein (GFAP)–IR (Fig. S1 F), which label dendritic spines and reactive astrocytes, respectively. This suggests that entorhinal neurons also represent a possible presynaptic source of BDNF for CA1 neurons.

Immunogold-labeled sections from both WT and *Bsn* mutants were then examined at 2,000-fold magnification. In comparison with CON animals (Fig. 8, A and B), a higher number of labeled MFB profiles containing more BDNF-positive DCVs was observed in sections from *Bsn* mutants (Fig. 8, C and D), with clusters accumulated at the synaptic membrane. This was confirmed by quantification, with anti-BDNF–labeled MFBs containing a significantly higher density of gold clusters (1.7 ± 0.3 clusters/μm^2; Fig. 8 E) and grains (14.4 ± 2.5 grains/μm^2; Fig. 8 F) compared with CONs (0.8 ± 0.01 clusters/μm^2 with $P < 0.05$ and 6.9 ± 0.5 grains/μm^2 with $P < 0.05$, respectively). Similarly, anti–pro-BDNF–labeled profiles from *Bsn* mutants also displayed a higher density of gold clusters (2.02 ± 0.27 clusters/μm^2;

Fig. 8 E) and grains (17.2 ± 2.8 grains/μm^2; Fig. 8 F) compared with CON profiles (0.96 ± 0.04 clusters/μm^2 with $P < 0.005$ and 10.1 ± 0.9 grains/μm^2 with $P < 0.05$, respectively); these relatively low increases in mean cluster densities are a result of the larger areas of MFB profiles in *Bsn* mutants.

Gold grain distribution and density in dendrites were also compared between *Bsn* mutant (Fig. 9, C and D) and CON tissues (Fig. 9, A and B). Dendritic profiles were again scrutinized for evidence of labeled vesicles, but none was found in tissues from either group. Density measurements revealed background values in *Bsn* mutant mice similar to those observed in CON mice, both in tissues labeled with anti-BDNF (5.4 ± 0.4 grains/μm^2 for *Bsn* mutant vs. 5.7 ± 0.5 grains/μm^2 for CON; $P = 0.66$; Fig. 9 E, left) and anti–pro-BDNF (5.1 ± 0.1 grains/μm^2 for *Bsn* mutant vs. 6.3 ± 0.3 grains/μm^2 for CON; $P = 0.12$; Fig. 9 E, right). Increased labeling density was not detected in the extracellular space or in nonneuronal cell types such as astrocytes.

Verification of background immunogold labeling

To determine whether background gold labeling is evenly distributed over different subcellular compartments, we extended the quantitative gold grain analysis to dendritic spine profiles and myelinated axon profiles in SL, as they are devoid of cluster-labeled organelles. Quantification of single gold grains overlying these profiles revealed that the density of background gold labeling depends on the type of subcellular compartment (Table 1). The mean values for gold grain densities in spine and myelinated axon profiles did not differ between WT/Myc versus *cbdnf ko* or WT versus *Bsn* mutant tissues. Therefore, spines and myelinated axons from WT mice do not exhibit anti-BDNF and anti–pro-BDNF immunogold labeling above the background levels observed in *cbdnf ko* tissues, nor do they contain specifically labeled organelles.

Biochemical detection and quantification of the BDNF pro-peptide

The identity of the molecules recognized by the BDNF antibodies in the immunochemistry experiments was then determined
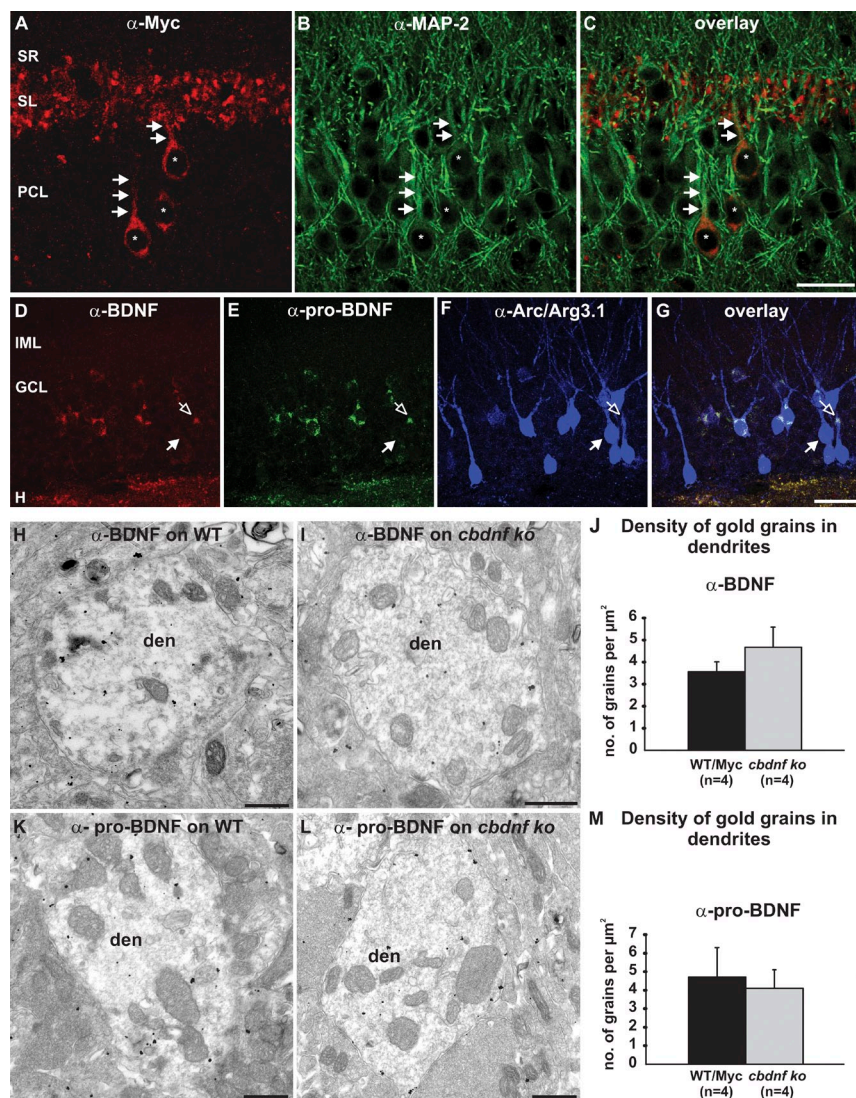
Figure 6. **BDNF-IR does not extend beyond proximal dendrites.** (A) Myc-IR in the CA3 region showing immunoreactive neuronal somata (asterisks) in the pyramidal cell layer (PCL) and Myc-positive MFB profiles in SL. (B) Anti–MAP-2 staining showing the distribution of pyramidal cell dendrites in CA3. (C) The merged image confirms that Myc-IR is preferentially confined to cell bodies in the pyramidal cell layer and presynaptic terminals in SL. (A–C) Arrows denote limited Myc-IR in proximal apical dendrites. (D–F) High-resolution confocal stack of the DG labeled with antibodies against BDNF (D), pro-BDNF (E), and Arc/Arg3.1 (F). The filled arrows label Arc/Arg3.1-positive, BDNF-negative cells, and the open arrows show BDNF-positive, Arc/Arg3.1-negative cells. GCL, granule cell layer; H, hilus; IML, inner molecular layer. (G) The merged image demonstrates that the majority of granule cells expressing BDNF-IR and pro-BDNF–IR also show Arc/Arg3.1-IR. (H–M) Nonspecific BDNF and pro-BDNF immunogold labeling in dendrites (den). In WT sections labeled with BDNF (H) or pro-BDNF (K) antibodies, gold grains are distributed throughout the dendrites but do not label any specific organelles. In *cbdnf ko* sections labeled with the same antibodies, a similar gold grain distribution to WT dendrites is observed for both BDNF (I) and pro-BDNF (L) antibodies. Quantification of gold grain density in dendrites reveals no difference between pooled WT/*Bdnf-Myc* versus *cbdnf ko* tissues labeled with either BDNF (J) or pro-BDNF (M) antibodies. Error bars represent SEM. Bars: (A–G) 30 µm; (H, I, K, and L) 500 nm.

using hippocampal lysates from WT and mutant mice (*cbdnf ko* and *Bsn*). Immunoprecipitates were analyzed by Western blotting (WB) and probed with either the BDNF polyclonal antibody N-20 or the monoclonal antibody 5H8, which recognizes an epitope in the prodomain of BDNF (Fig. 1 A). These experiments revealed the presence not only of pro-BDNF ($\sim$32 kD) but also of the much more abundant pro-peptide ($\sim$17 kD; Fig. 10 A; also see Fig. 1 A). Both signals were absent in lysates from *cbdnf ko* animals (Fig. 10 A). Quantification of the corresponding signal intensities revealed that the ratio of pro-peptide versus pro-BDNF is $\sim$10.3 ± 2.0 (n = 3; Fig. 10 B), similar to that of BDNF versus pro-BDNF (11 ± 2.0; n = 3; Fig. 10, B and C). A similar analysis of hippocampal lysates from *Bsn* mutants confirmed an approximate threefold increase each in BDNF, its pro-peptide, and pro-BDNF in mutant tissues (Fig. 10 C). These results also indicate that the respective ratios of BDNF and the pro-peptide versus pro-BDNF are similar to what is observed in WT animals. Of note is that the consistent detection of BDNF pro-peptide was only possible after glutaraldehyde fixation of the transfer membrane (see Materials and methods). Furthermore, under the lysate

and incubation conditions used, no measurable proteolysis of recombinant pro-BDNF (500 pg) added to the lysates at the beginning of the extraction procedure could be detected (Fig. S2). The recovery of added recombinant pro-BDNF was 102.2 ± 5.8% (n = 4).

Discussion

Our study reveals that in the adult hippocampus, BDNF and its cleaved pro-peptide are stored in large DCVs located in the presynaptic terminals of excitatory neurons. Both in WT and *Bsn* mutant mice, BDNF and its pro-peptide are stored at roughly equimolar ratios and are $\sim$10-fold more abundant than pro-BDNF in hippocampal lysates. Together with the lack of any detectable BDNF staining in dendrites or spines, our results provide direct support for an anterograde mode of action for BDNF in the intact CNS. They also offer a morphological substrate for recent findings indicating that the release of endogenous BDNF accounts for some of the rapid calcium transients observed at synaptic sites on dendrites of CA3 neurons (Lang et al., 2007).

Figure 7. Elevated BDNF staining in *Bsn* mutants. (A–D) Representative images from CON tissues showing anti-BDNF labeling in the DG (A) and CA3 area (C) and anti–pro-BDNF–Mab5H8 labeling in the DG (B) and CA3 (D). GCL, granule cell layer; H, hilus; IML, inner molecular layer; PCL, pyramidal cell layer. Overall distribution and staining intensities highly resemble those described for WT and *Bdnf-Myc* animals in Fig. 2. (E–H) In the corresponding regions of *Bsn* mutant sections, BDNF- and pro-BDNF–Mab5H8-IR are markedly increased in the hilus of the DG (E and F) as well as in SL (G and H). Note that lack of proportional increase in staining in the associated cell layers, namely the GCL (E and F) and pyramidal cell layer of CA3 (G and H). (I and J) High-power examination of the GCL reveals numerous albeit weakly labeled BDNF-positive (I) and pro-BDNF–Mab5H8-positive (J) granule cells, with labeling confined to the cell soma and no detectable dendritic staining in the inner molecular layer. (K and L) In SL of *Bsn* mutants, an increased density of labeled profiles was observed, with BDNF-IR (K) and pro-BDNF–IR-Mab5H8 (L) showing virtually no overlap with the postsynaptic markers synpo (green; K) and MAP-2 (red; L), respectively. Bars: (A–H) 100 µm; (I and J) 30 µm; (K and L) 15 µm.
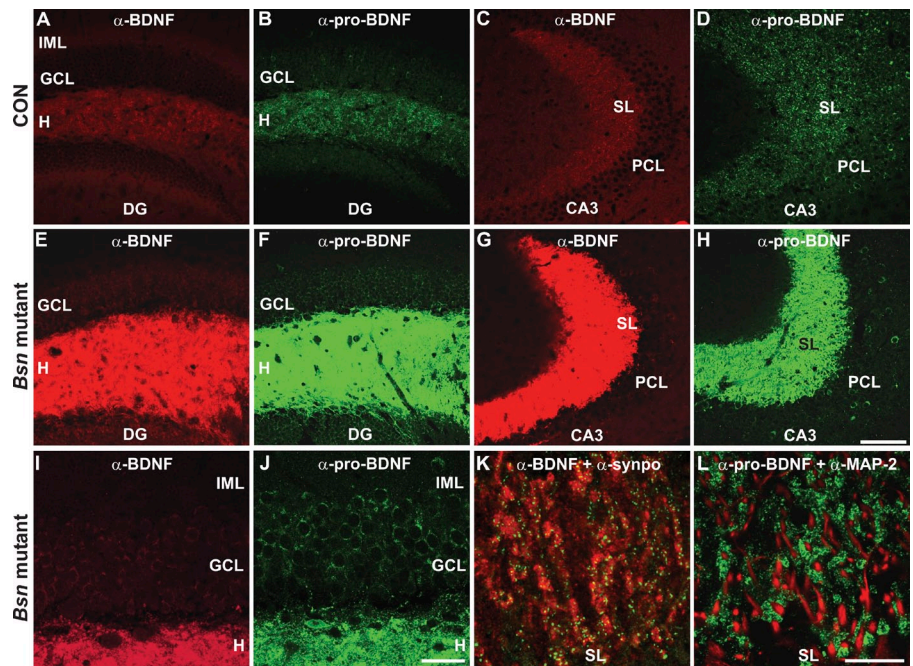
## Immunohistochemical localization of BDNF in the CNS

The specificity of BDNF immunostaining in the adult brain is very difficult to ascertain, as *Bdnf* knockout animals die before reaching maturity, a fact that complicates the interpretation of previous immunohistochemical studies (Wetmore et al., 1991; Dugich-Djordjevic et al., 1995; Schmidt-Kastner et al., 1996; Altar et al., 1997; Conner et al., 1997; Yan et al., 1997; Luo et al., 2001; Danzer and McNamara, 2004; Tongiorgi et al., 2004; Zhou et al., 2004; Agassandian et al., 2006; Avwenagha et al., 2006, Salio et al., 2007). Our study deals with the mature hippocampus, as much of the current interest in BDNF relates to its role in the adult brain, and the staining specificity of our BDNF monoclonal antibody was verified with tissues from age-matched mice lacking BDNF in the CNS (Kolbeck et al., 1999; Rauskolb et al., 2010). The choice of BDNF antibody was also important, as none of the commercially available BDNF antibodies we tested yielded specific staining (unpublished data). In addition, a mouse line was used in which *Bdnf* was replaced with a Myc-tagged version of the gene (Matsumoto et al., 2008), allowing additional control experiments to be performed with anti–human Myc antibodies on WT tissue sections. We note that a recent light microscopy study that also used a knockin strategy to tag endogenous BDNF came to a conclusion very similar to our own, revealing identical labeling of the mossy fiber pathway with antibodies directed against either the HA epitope used to tag BDNF or the BDNF prodomain (Yang et al., 2009). However, our biochemical results (see later part of Discussion) now indicate that pro-BDNF antibodies primarily detect the BDNF pro-peptide, which is present at much higher levels than uncleaved pro-BDNF. The pro-BDNF antibodies further validate our localization data, as they recognize an epitope unrelated to those detected by the antibodies to BDNF or Myc but similarly label presynaptic large DCVs. These organelles are well known

to be involved in the regulated secretion of many other neuronal signaling peptides including Met-enk (Cheng et al., 1995), which was also used here as a presynaptic marker. DCVs are typically found in presynaptic terminals but rarely in postsynaptic structures such as dendrites or spines, with the notable exception of the DCVs containing the neuropeptides vasopressin and oxytocin, found in the dendrites of specialized neurosecretory cells (Kennedy and Ehlers, 2011).

Using cultured cells to study the cell biology of BDNF

Numerous previous studies have used cultured hippocampal neurons to study the storage and release of BDNF (Haubensak et al., 1998; Hartmann et al., 2001; Wu et al., 2004; Adachi et al., 2005; Brigadski et al., 2005; An et al., 2008; Dean et al., 2009; Matsuda et al., 2009). They all come to the conclusion that BDNF is stored in and released from both axonal and dendritic compartments, raising the question of what could underlie the apparent discrepancy with our findings. Although the majority of these studies utilize neurons transfected with a cDNA encoding a fluorescently tagged form of BDNF, some of the conclusions are also based on the detection of endogenous BDNF in vitro. However, cultured embryonic neurons grow in a very different environment compared with neurons in vivo, with fewer and less intimate cell–cell interactions between neighboring neurons and astrocytes, an incomplete ECM, and a lack of laminar input. In vivo, the development of neuronal circuits is spatially tightly regulated (Frotscher et al., 2000), whereas in vitro, synapses seem to form randomly. As a result of these cell-extrinsic differences, it is conceivable that cultured neurons fail to sort cargo-loaded vesicles as strictly as they do in vivo (Mellman and Nelson, 2008). In addition, we note that cultured neurons express significantly higher levels of BDNF than are detectable even in adult hippocampal extracts (unpublished data).
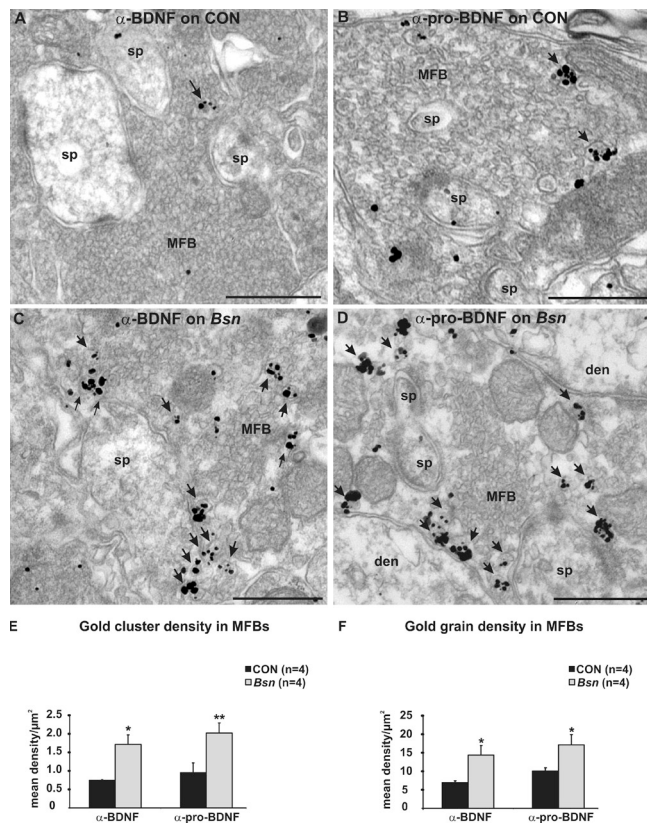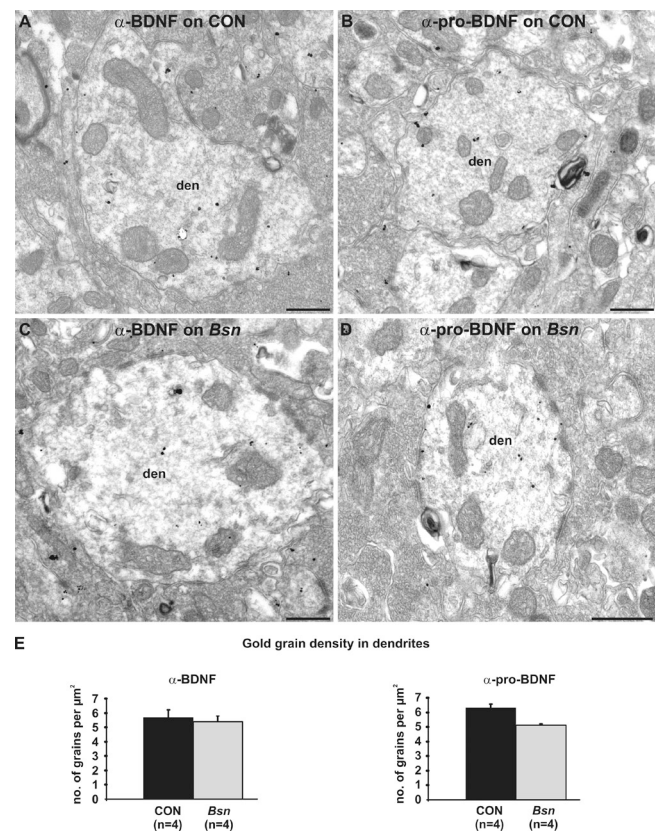
Figure 8. **Higher density of BDNF-positive DCVs in MFBs of *Bsn* mutant animals.** (A and B) Electron micrographs of MFBs from CON sections prelabeled with BDNF (A) or pro-BDNF (B) immunogold. Gold cluster–labeled secretory vesicles were occasionally observed in a subset of terminals (arrows). sp, dendritic spine. (C and D) In MFBs from *Bsn* mutants, there was an increase in the number of cluster-labeled vesicles (arrows) as well as single gold grains, both in the case of BDNF (C) and pro-BDNF (D) immunogold. den, dendrite. (E and F) This was confirmed by quantification. Error bars represent SEM. Bars, 500 nm.

Figure 9. **BDNF is not targeted to dendrites in *Bsn* mutants.** (A–E) Comparison of dendrites (den) in SL in CON (A and C) versus *Bsn* mutant tissues (B and D) revealed a lack of difference in the density of gold grains, both in the case of BDNF immunogold (E, left) and pro-BDNF immunogold (E, right). Also note the general absence of DCVs within dendritic profiles of both CON and *Bsn* mutant animals. Error bars represent SEM. Bars, 500 nm.

BDNF biosynthesis and processing

Although in situ hybridization experiments have long established that BDNF mRNA can be unambiguously detected in the cell bodies of excitatory neurons (Hofer et al., 1990; Isackson et al., 1991), some studies have also suggested its presence in dendrites (Tongiorgi et al., 1997, 2004; An et al., 2008) and its active transport upon stimulation (Tongiorgi et al., 1997, 2004; Chiaruttini et al., 2009; Baj et al., 2011; Louhivuori et al., 2011; Wu et al., 2011). However, these experiments revealed that BDNF mRNA is predominantly detected in the most proximal part of the dendrite, whereas other actively transported mRNAs can be detected in dendrites hundreds of micrometers away from the soma, as is the case for the Arc/Arg3.1 (Lyford et al., 1995), CaMKII-α (Burgin et al., 1990; Miller et al., 2002), or dendrin (Link et al., 1995) mRNAs. This leaves the possibility that BDNF mRNA localizes to proximal dendrites by diffusion rather than active transport. Selective trafficking has also been difficult to assess, as activity-dependent transcription augments the intensity of the proximal mRNA signal, allowing more distal diffusion of the in situ hybridization enzymatic reaction product (Tongiorgi et al., 1997, 2004). Although elegant experiments aimed at blocking protein synthesis and interfering with

BDNF signaling have inferred the translation of BDNF mRNA in dendrites (Tanaka et al., 2008), it has not been possible thus far to assess directly whether dendritic BDNF mRNAs are translated locally. Thus, it is of particular significance that our experiments revealed a complete lack of specific BDNF protein signals in dendrites not only in WT but also in *Bsn* mutant animals. Although our experiments cannot rule out that functionally relevant quantities of BDNF may be released from dendrites, they indicate that, at present, there is no structural basis for this speculation.

With regard to the biochemistry of BDNF, initial studies suggested that the most abundant, or indeed the only detectable, translation product in adult brain extracts was uncleaved pro-BDNF (Chen et al., 2005; An et al., 2008). However, a signal of similar size and intensity to pro-BDNF can readily be detected in mice lacking BDNF in the CNS (Matsumoto et al., 2008). Furthermore, pulse-chase experiments showed that pro-BDNF is a short-lived intermediate that is rapidly processed intracellularly (Matsumoto et al., 2008). BDNF, like all other neurotrophins, is initially translated as a glycosylated precursor protein, presumably allowing the proper folding and disulfide bridging of the mature protein (Leibrock et al., 1989; Rattenholl et al., 2001). Accordingly, we detected specific pro-BDNF–IR in the

Table 1. **Comparative gold grain densities in subcellular compartments devoid of cluster-labeled organelles**

Subcellular profile	Anti-BDNF immunogold				Anti–pro-BDNF immunogold			
	WT/Myc	cbdnf ko	CON	Bsn	WT/Myc	cbdnf ko	CON	Bsn
	n = 3	n = 3	n = 4	n = 4	n = 3	n = 3	n = 4	n = 4
Dendrite[a]	3.6 ± 0.5	4.7 ± 0.9	6.9 ± 0.9	6.6 ± 0.7	4.7 ± 1.6	4.1 ± 1.5	6.3 ± 0.3	5.1 ± 0.1
Spine	19.3 ± 2.1	18.4 ± 3.8	15.0 ± 1.4	13.1 ± 0.9	18.2 ± 1.2	20.3 ± 4.5	13.8 ± 0.6	14.3 ± 1.6
Myelinated axon	9.6 ± 1.8	11.6 ± 0.7	8.3 ± 0.5	8.1 ± 1.2	12.2 ± 0.8	10.7 ± 0.7	8.5 ± 1.1	10.1 ± 1.5

Two-sided t tests for all profiles in both anti-BDNF immunogold and anti–pro-BDNF immunogold were $P > 0.05$. All values expressed as the group mean value ± SEM
n value correspond to the number of animals examined per experiment. Subcellular profiles are represented as no. of grains/μm^2.
[a]Gold grain densities in dendrites are also presented in graph form in Fig. 6 (WT/Myc vs. cbdnf ko) and Fig. 9 (CON vs. Bsn mutant).

Golgi apparatus of dentate granule cells and CA3 neurons but not in other organelles such as lysosomes or endosomes. Although the intracellular site of pro-BDNF cleavage and the participating proteases are yet to be identified, the existence of the BDNF pro-peptide in brain lysates has not been previously reported (see Fig. 10). This pro-peptide has hitherto escaped detection presumably because it is readily washed away from blotting membranes. This loss could be prevented by fixing the membranes with glutaraldehyde after electrophoretic transfer (Karey and Sirbasku, 1989). Although we observed that prolonged stimulation of cultured neurons results in the cosecretion of BDNF and its pro-peptide (unpublished data), the biological significance of this corelease is unclear.

### BDNF detection in the hippocampus of *Bsn* mutants

Mutant mice expressing a truncated version of the large presynaptic protein Bassoon develop spontaneous epileptic seizures for reasons that are only partially understood (Altrock et al., 2003). In line with the well-established link between excitatory neuronal activity and *Bdnf* transcription, BDNF protein levels were found to increase in parallel with, but not precede, the development of seizure episodes (Heyden et al., 2011). It seems unlikely that Bassoon is directly involved in the increase in BDNF levels, as a mutation in the potassium channel Kv1.1 that also leads to seizure activity is accompanied by a marked increase in BDNF mRNA and megencephaly (Diez et al., 2003; Lavebratt et al., 2006), as is the case

for the *Bsn* mutation (Angenstein et al., 2007). Blocking activity with carbamazepine in the Kv1.1 mutant prevents the development of megencephaly and restores BDNF mRNA to normal levels (Lavebratt et al., 2006). Despite the marked increase in BDNF and its pro-peptide in the *Bsn* mutant, both immunoreactive signals remained confined to presynaptic terminals, with no detectable staining in either granule or pyramidal cell dendrites or glial cells (Bergami et al., 2008). In comparison with WT animals, the only remarkable change observed in the *Bsn* mutant was an increase in the density of BDNF-positive DCVs in MFBs. These observations are in line with earlier studies in the rat, in which chemically induced seizure activity led to an increase in presynaptic BDNF staining (Vezzani et al., 1999; Scharfman et al., 2002; Danzer and McNamara, 2004). Despite the substantially higher BDNF levels, we did not detect any BDNF staining in the extracellular space, suggesting that after its release, BDNF becomes rapidly diluted by diffusion as well as by cellular reuptake, thus preventing accumulation to a degree that would allow immunohistochemical detection.

BDNF and hippocampal mossy fibers

The hippocampal mossy fiber projection stands out as the most heavily stained structure in the adult CNS using either BDNF or pro-BDNF antibodies (Fig. 1). This pathway is thought to exhibit presynaptic long-term potentiation (LTP; Nicoll and Schmitz, 2005) and to be important for pattern completion as well as for the storage and recall of information

Figure 10. **Biochemical detection of BDNF, its pro-peptide, and pro-BDNF.** IP of hippocampal lysates (500 µg) was performed either with an anti–pro-BDNF antiserum or with the BDNF antibody followed by WB with the antibodies indicated. (A) Both pro-BDNF and its pro-peptide were detected in WT (first lane) but not in cbdnf ko samples (second lane). Similar results were obtained using the pro-BDNF antibody AN-03 in IP and/or WB (not depicted). HIP, hippocampus; IB, immunoblot; non-glyc., nonglycosylated; rec., recombinant. (B) Note that the ratio of pro-peptide to pro-BDNF is similar to that of BDNF and pro-BDNF (n = 3). Error bars represent the SEM of the three samples measured. (C) IP/WB analysis of hippocampal lysates from Bsn mutants reveals a relatively similar increase (approximately threefold) in the levels of BDNF and pro-BDNF (left, second lane) as well as pro-peptide and pro-BDNF (right, second lane) compared with CON tissues (left and right, first lanes). Recombinant BDNF pro-peptide and cleavage-resistant pro-BDNF were used as molecular mass markers.
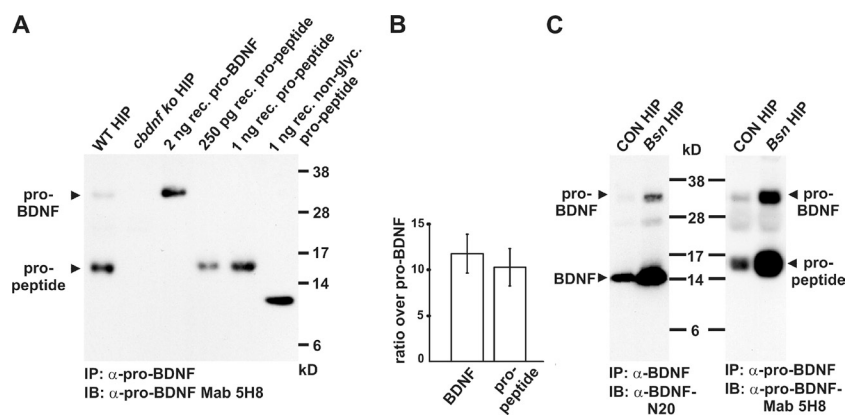
(Bischofberger et al., 2006; Kerr and Jonas, 2008). Recent studies have also shown that long-term experience results in rearrangements of presynaptic MFBs (Galimberti et al., 2006, 2010; Rekart et al., 2007) and that LTP induction results in a dramatic increase in MFB profile size accompanied by postsynaptic spine growth and de novo formation of release sites (Zhao et al., 2012). Although it remains to be demonstrated that presynaptic release of BDNF is involved in these morphological changes, endogenous BDNF signaling has been shown to account for some of the spontaneous, rapid calcium transients observed at synaptic sites on CA3 dendrites (Lang et al., 2007). In addition, θ-burst–induced release of endogenous BDNF from mossy fibers is sufficient to induce intracellular changes in postsynaptic CA3 neurons (Li et al., 2010). Furthermore, several previous studies in CA1 have pointed to the need for BDNF in order for LTP to reach maximal values (Korte et al., 1995; Patterson et al., 1996), and our results uncover a presynaptic location of BDNF in this hippocampal area (Figs. 5 and S1).

Conclusion

Our localization data provide a structural substrate for previous functional results, suggesting that BDNF exerts its action on postsynaptic CNS neurons primarily in an anterograde fashion (Altar et al., 1997; Zakharenko et al., 2003; Baquet et al., 2004). This mode of action is the converse of the long-established model based on NGF in the peripheral nervous system, whereby neurotrophins are released from various cell types, including smooth muscle cells, and then act retrogradely on presynaptic neurons. Together with the recent discovery that the NGF receptor TrkA causes neuronal death in the absence of its ligand, whereas the BDNF receptor TrkB does not (Nikoletopoulou et al., 2010), these results suggest profound differences in the biology and directionality of growth factor signaling between the peripheral nervous system and the CNS.

Materials and methods

Mouse lines
Brains were obtained from the following lines of mice, all of which were used at ~8 wk of age: WT (C57Bl6), *Bdnf-Myc* (Matsumoto et al., 2008), *cbdnf ko* (Rauskolb et al., 2010), and *Bsn* mutant (*BsnΔEX4/5*; Altrock et al., 2003). All experiments were performed in accordance with the institutional guidelines of the University of Freiburg and the University of Basel.

Preparation of tissue for immunostaining
Mice (n = 7 for WT, n = 7 for *Bdnf-Myc*, n = 4 for *cbdnf ko*, and n = 7 for *Bsn* mutant) were transcardially perfused with 0.9% NaCl followed by a mixture of 4% PFA, 0.1% glutaraldehyde, and 0.3% picric acid in 0.1 M phosphate buffer (PB), pH 7.4. Brains were removed and postfixed with 4% PFA in 0.1 M PB for 1 h before thorough washing in 0.1 M PB. Coronal sections (50 µm) of the hippocampus were cut on a vibratome (Leica) and collected in 0.1 M PB. Sections along the septotemporal axis of the hippocampus were further processed either for immunofluorescent labeling or preembedding immunogold labeling.

Antibodies for immunostaining
BDNF was detected with the mouse monoclonal anti-BDNF antibody Mab#9 (anti-BDNF; Kolbeck et al., 1999) directed against the mature domain of BDNF (see Fig. 1 A). This antibody also recognizes the uncleaved form of BDNF, i.e., pro-BDNF (Fig. 1 A; Matsumoto et al., 2008). *BDNF-Myc* was detected with goat polyclonal c-Myc antibodies (anti-Myc; SC-789; Santa Cruz Biotechnology, Inc.). Pro-BDNF was detected with a rabbit

polyclonal antibody (anti–pro-BDNF; #ANT-006, batch AN-03; Alomone Labs) raised against the prodomain of BDNF protein (see Fig. 1 A). To determine whether the signals obtained with anti–pro-BDNF could also be observed with other antibodies against the prodomain of BDNF, we tested a commercially available mouse monoclonal pro-BDNF antibody (anti–pro-BDNF–Mab5H8; SC-65514; Santa Cruz Biotechnology, Inc.). The staining pattern produced by this antibody (as specified in the figure legends) was comparable with the results obtained with the polyclonal anti–pro-BDNF. Presynaptic components were detected with mouse monoclonal antibodies against the vesicular glutamate transporter 1 (anti–VGLUT-1; #135511; Synaptic Systems) and rabbit polyclonal antibodies against SYP (anti-SYP; Santa Cruz Biotechnology, Inc.); for postsynaptic labeling, mouse monoclonal antibodies against MAP-2 (anti-MAP-2; #M2320; Sigma-Aldrich), rabbit polyclonal antibodies against the spine apparatus protein synpo (anti-synpo; #S9567; Sigma-Aldrich), and guinea pig polyclonal antibodies against activity-related cytoskeletal protein (anti-Arc/Arg3.1; #156005; Synaptic Systems) were used. A mouse monoclonal antibody against the 130-kD Golgi matrix protein (anti-GM130) was used for the detection of the Golgi complex (#610822; BD). For labeling of neuropeptides within the mossy fiber projection, rabbit polyclonal antibodies against Met-enk (anti–Met-enk; Millipore) and CCK (anti-CCK; #P06307; Millipore) were used. Astrocytes were detected with a guinea pig polyclonal antibody serum against GFAP (anti-GFAP; #031223; Advanced ImmunoChemical Inc.).

Immunofluorescence
As preliminary staining experiments with anti-Myc antibodies yielded high levels of nonspecific staining in sections from WT mice, the Myc antibody solution was preincubated with WT sections, and the solution was subsequently used to stain sections from *Bdnf-Myc* and WT mice. Except for this first blocking step, the staining protocol for all antibodies was identical, and TBS, pH 7.4, was used throughout to wash the sections. For staining with polyclonal antibodies, sections were blocked with 20% normal donkey serum in TBS for 1 h; for staining with monoclonal antibodies, sections were blocked with 3% M.O.M (Mouse-on-Mouse blocking serum; Vector Laboratories) in TBS for 1 h. Primary antibodies were diluted in a solution of 3% BSA, 2% normal donkey serum, and 0.2% Triton X-100 in TBS to yield the following final concentrations/dilutions: 10 µg/ml anti-BDNF, 0.4 µg/ml anti-Myc, 1.33 µg/ml anti–pro-BDNF, 3.3 µg/ml anti–VGLUT-1, 4 µg/ml anti-SYP, 0.9 µg/ml anti-GM130, 2 µg/ml anti-Arc/Arg3.1, 4 µg/ml anti–MAP-2, 1:2,000 anti-synpo, 3 µg/ml anti–Met-enk, 1:2,000 anti-CCK, and 1:1,000 anti-GFAP. Sections were incubated for at least one night at 4°C in either one or more of these primary antibodies. For fluorescent signal detection, the following Alexa Fluor–conjugated secondary antibodies were used: donkey anti–rabbit-488 or -555, donkey anti–goat-555 or -488, donkey anti–mouse-555 or -647, and donkey anti–guinea pig–Cy5 (all purchased from Millipore). Labeled sections were mounted onto glass slides and coverslipped with fluorescent mounting medium (Dako).

Confocal microscopy
Slide-mounted sections of immunolabeled hippocampi were viewed on an inverted microscope (Axiovert 200; Carl Zeiss) equipped with Plan Apochromat 20× (0.75 NA) or 63× (oil differential interference contrast; 1.4 NA) objectives and attached to a spectral confocal laser system (LSM 510; Carl Zeiss) powered by LSM 4.2 Meta software (Carl Zeiss). The tissue was scanned at room temperature with 488-, 543-, and 633-nm laser lines to detect the Alexa fluorophores 488, 555, and 647, respectively, and high-resolution images of optical sections (z slices) were captured using sequential line (mean of four) scanning. Colocalization of two or three fluorophores was qualitatively assessed in the x, y, and z planes of each optical section. Maximal projection images of confocal z series (stacks) were generated where indicated in the figure legends. Minimal adjustments to image contrast and intensity were made in Photoshop CS (version 8.0.1; Adobe) using the levels or contrast/brightness functions. Images were arranged and annotated using CorelDRAW 12 software (Corel Corporation).

Immunogold EM
Immunogold prelabeling. 50-µm vibratome sections of perfusion-fixed hippocampi from WT, *Bdnf-Myc*, *cbdnf ko*, and *Bsn* mutant mice were thoroughly washed in 50 mM TBS, pH 7.4, and immersed for 2 h in a cryoprotecting solution (25% sucrose and 10% glycerol in 0.05 M PB) before being snap frozen in liquid nitrogen–cooled isopentane. After immediate thawing and washing in 0.1 M PB, sections were incubated for 1 h in blocking solution (3% M.O.M. in TBS for anti-BDNF staining and 20% normal goat serum in TBS for anti–pro-BDNF and anti-Myc staining)

followed by one to three nights at 4°C in a 3% BSA/TBS solution containing either 20 µg/ml anti-BDNF, 1.33 µg/ml anti–pro-BDNF (AN-03), or 0.4 µg/ml anti-Myc antibody. After thorough washing in TBS, the sections were incubated overnight at 4°C in 3% BSA/TBS solution containing either 1.4 nm of gold-conjugated goat anti–mouse, goat anti–rabbit, or rabbit anti–goat IgG. Sections were rinsed in TBS and then fixed for 10 min in a 1% glutaraldehyde solution. Tissue-bound gold particles were enlarged using a silver intensification kit (HQ Silver; Nanoprobes). The sections then underwent osmification for 40 min in a solution of 0.5% OsO_4 and 6.86% sucrose in 0.1 M PB.

Embedding. After osmification, sections were washed in 0.1 M PB followed by 50% ethanol (EtOH). The tissue was then incubated in 1% uranyl acetate in 70% EtOH for 35 min followed by 10-min dehydration steps in increasing grades of EtOH. After washing in propylene oxide, the tissue was embedded in Durcupan (Fluka). Ultrathin sections (60 nm) of selected hippocampal areas (DG, CA3, and CA1) were cut and mounted on formvar-coated nickel grids. Sections were viewed and examined in an electron microscope (LEO 906E; Carl Zeiss).

Quantification of immunogold staining

Gold-labeled sections from WT, *Bdnf-Myc*, *cbdnf ko*, and *Bsn* mutant animals were first examined in the electron microscope at magnifications ranging from 6,000 to 12,000×, and areas containing labeled structures in SL of CA3 were then photographed using a dual-speed charge-coupled device camera (TRS SharpEye; Troendle) and analySIS acquisition software (Soft Imaging System; Olympus). MFBs were unambiguously identified based on their well-defined morphology (see criteria in Results). An organelle in an MFB was deemed labeled if associated with at least four gold grains (described in this study as a cluster). MFBs containing labeled organelles were then selected for quantitative analysis, in which the number of clusters per bouton profile was manually counted, and the area and perimeter of each profile were simultaneously measured with cell^P software (Soft Imaging System). The number of clusters per bouton was then reexpressed as a density measurement (i.e., the number of clusters per µm² of MFB). Although the rare gold clusters observed in *cbdnf ko* sections showed no association with any particular organelle, they were still included in the counts. In addition to cluster quantification, the respective number of single gold grains in MFBs from WT, *Bdnf-Myc*, *cbdnf ko*, and *Bsn* mutant tissues was also determined and ultimately expressed as a density measurement (i.e., the number of grains per µm² of MFB).

For quantification of gold labeling in dendritic profiles, an initial qualitative analysis of the tissue revealed a complete lack of cluster-labeled organelles, including large secretory vesicles and endosomes. Therefore, to compare gold grain density in dendrites from different groups of animals, the number of single gold grains per dendritic profile was counted and expressed in relation to the area of the corresponding profile (i.e., the number of grains per µm²).

Finally, to determine whether background gold grain labeling was equally distributed across different subcellular compartments, the quantitative gold grain analysis was extended to two additional compartments in SL, namely dendritic spine profiles and myelinated axon profiles. These two compartments were chosen on the basis of also being devoid of cluster-labeled organelles.

Immunoprecipitation (IP) and WB

Hippocampi were dissected from 8-wk-old WT, *cbdnf ko*, and *Bsn* mutant mice and then weighed and stored at −80°C. 10 vol/wt of radioimmunoprecipitation assay buffer (50 mM Tris-HCl, pH 7.4, 150 mM NaCl, 1 mM EDTA, 1% Triton X-100, and 0.2% Na deoxycholate) was added. To prevent proteolysis, freshly prepared protease inhibitors including a protease inhibitor cocktail (Roche), 10 µM 1,10-phenanthroline monohydrate, 10 mM 6-aminohexanoic acid, and 10 µg/ml aprotinin were added to the buffer. The tissues were sonicated, the homogenates centrifuged, and the supernatants collected. IP was performed with 500 µg of total protein using either the BDNF monoclonal antibody Mab#9 or a rabbit polyclonal antibody raised against the BDNF pro-peptide (Koshimizu et al., 2009) in the presence of protein G agarose (Roche) according to the manufacturer's instructions. After blotting, the proteins were fixed to the membrane with 0.5% glutaraldehyde for 30 min at room temperature and probed with either polyclonal rabbit anti-BDNF N20 (sc-546; Santa Cruz Biotechnology, Inc.) or monoclonal mouse anti–pro-BDNF Mab5H8 (1:200) using an IP Western kit (GenScript) to eliminate nonspecific signals from protein G. Signal intensity measurements were performed using ImageJ software (National Institutes of Health). Recombinant WT and cleavage-resistant pro-BDNF (Fayard et al., 2005) as well as the mouse BDNF pro-peptide

were produced in COS7 cells transfected with the corresponding cDNAs cloned in plasmid cytomegalovirus vectors. The concentrations of these proteins were then determined against known amounts of purified BDNF pro-peptide produced in *Escherichia coli* (Koshimizu et al., 2009). The COS7-derived cleavage-resistant pro-BDNF was used as a molecular mass marker, whereas WT pro-BDNF was used in recovery experiments with tissue lysates (Fig. S2)

Statistical analysis

All values are expressed as mean ± SEM. For BDNF and pro-BDNF immunogold quantification, 10–20 MFBs and 30–40 dendrites per WT, *Bdnf-Myc*, *cbdnf ko*, and *Bsn* mutant mice were analyzed, and mean values for each animal were calculated. Group means (pooled WT/*BDNF-Myc* vs. *cbdnf ko* and WT vs. *Bsn* mutant) were compared using a two-sided Student's *t* test. A probability of $P < 0.05$ was considered to be statistically significant.

Online supplemental material

Fig. S1 shows an increase in BDNF-IR and pro–BDNF-IR in area CA1 of the Bassoon mutant hippocampus. Fig. S2 shows the complete recovery of WT recombinant pro-BDNF from hippocampal lysates. Online supplemental material is available at http://www.jcb.org/cgi/content/full/jcb.201201038/DC1.

References

Adachi, N., K. Kohara, and T. Tsumoto. 2005. Difference in trafficking of brain-derived neurotrophic factor between axons and dendrites of cortical neurons, revealed by live-cell imaging. *BMC Neurosci.* 6:42. http://dx.doi.org/10.1186/1471-2202-6-42

Agassandian, K., M. Gedney, and M.D. Cassell. 2006. Neurotrophic factors in the central nucleus of amygdala may be organized to provide substrates for associative learning. *Brain Res.* 1076:78–86. http://dx.doi.org/10.1016/j.brainres.2006.01.009

Altar, C.A., N. Cai, T. Bliven, M. Juhasz, J.M. Conner, A.L. Acheson, R.M. Lindsay, and S.J. Wiegand. 1997. Anterograde transport of brain-derived neurotrophic factor and its role in the brain. *Nature.* 389:856–860. http://dx.doi.org/10.1038/39885

Altrock, W.D., S. tom Dieck, M. Sokolov, A.C. Meyer, A. Sigler, C. Brakebusch, R. Fässler, K. Richter, T.M. Boeckers, H. Potschka, et al. 2003. Functional inactivation of a fraction of excitatory synapses in mice deficient for the active zone protein bassoon. *Neuron.* 37:787–800. http://dx.doi.org/10.1016/S0896-6273(03)00088-6

Amaral, D., and P. Lavanex. 2006. Hippocampal Neuroanatomy. *In* The Hippocampus Book. P. Andersen, R. Morris, D. Amaral, T. Bliss, and J. O'Keefe, editors. Oxford University Press, Oxford. 37–114.

An, J.J., K. Gharami, G.Y. Liao, N.H. Woo, A.G. Lau, F. Vanevski, E.R. Torre, K.R. Jones, Y. Feng, B. Lu, and B. Xu. 2008. Distinct role of long 3' UTR BDNF mRNA in spine morphology and synaptic plasticity in hippocampal neurons. *Cell.* 134:175–187. http://dx.doi.org/10.1016/j.cell.2008.05.045

Angenstein, F., H.G. Niessen, J. Goldschmidt, H. Lison, W.D. Altrock, E.D. Gundelfinger, and H. Scheich. 2007. Manganese-enhanced MRI reveals structural and functional changes in the cortex of Bassoon mutant mice. *Cereb. Cortex.* 17:28–36. http://dx.doi.org/10.1093/cercor/bhj121

Avwenagha, O., M.M. Bird, A.R. Lieberman, Q. Yan, and G. Campbell. 2006. Patterns of expression of brain-derived neurotrophic factor and tyrosine kinase B mRNAs and distribution and ultrastructural localization of their proteins in the visual pathway of the adult rat. *Neuroscience.* 140:913–928. http://dx.doi.org/10.1016/j.neuroscience.2006.02.056

Baj, G., E. Leone, M.V. Chao, and E. Tongiorgi. 2011. Spatial segregation of BDNF transcripts enables BDNF to differentially shape distinct dendritic compartments. *Proc. Natl. Acad. Sci. USA.* 108:16813–16818. http://dx.doi.org/10.1073/pnas.1014168108

Baquet, Z.C., J.A. Gorski, and K.R. Jones. 2004. Early striatal dendrite deficits followed by neuron loss with advanced age in the absence of anterograde cortical brain-derived neurotrophic factor. *J. Neurosci.* 24:4250–4258. http://dx.doi.org/10.1523/JNEUROSCI.3920-03.2004

Bergami, M., S. Santi, E. Formaggio, C. Cagnoli, C. Verderio, R. Blum, B. Berninger, M. Matteoli, and M. Canossa. 2008. Uptake and recycling of pro-BDNF for transmitter-induced secretion by cortical astrocytes. *J. Cell Biol.* 183:213–221. http://dx.doi.org/10.1083/jcb.200806137

Bischofberger, J., D.M. Engel, M. Frotscher, and P. Jonas. 2006. Timing and efficacy of transmitter release at mossy fiber synapses in the hippocampal network. *Pflugers Arch.* 453:361–372. http://dx.doi.org/10.1007/s00424-006-0093-2

Brigadski, T., M. Hartmann, and V. Lessmann. 2005. Differential vesicular targeting and time course of synaptic secretion of the mammalian neurotrophins. *J. Neurosci.* 25:7601–7614. http://dx.doi.org/10.1523/JNEUROSCI.1776-05.2005

Burgin, K.E., M.N. Waxham, S. Rickling, S.A. Westgate, W.C. Mobley, and P.T. Kelly. 1990. In situ hybridization histochemistry of Ca2+/calmodulin-dependent protein kinase in developing rat brain. *J. Neurosci.* 10:1788–1798.

Calabrese, F., R. Molteni, P.F. Maj, A. Cattaneo, M. Gennarelli, G. Racagni, and M.A. Riva. 2007. Chronic duloxetine treatment induces specific changes in the expression of BDNF transcripts and in the subcellular localization of the neurotrophin protein. *Neuropsychopharmacology*. 32:2351–2359. http://dx.doi.org/10.1038/sj.npp.1301360

Cathomas, F., C. Vogler, J.C. Euler-Sigmund, D.J. de Quervain, and A. Papassotiropoulos. 2010. Fine-mapping of the brain-derived neurotrophic factor (BDNF) gene supports an association of the Val66Met polymorphism with episodic memory. *Int. J. Neuropsychopharmacol.* 13:975–980. http://dx.doi.org/10.1017/S1461145710000519

Chang, Q., G. Khare, V. Dani, S. Nelson, and R. Jaenisch. 2006. The disease progression of Mecp2 mutant mice is affected by the level of BDNF expression. *Neuron*. 49:341–348. http://dx.doi.org/10.1016/j.neuron.2005.12.027

Chen, Z.Y., A. Ieraci, H. Teng, H. Dall, C.X. Meng, D.G. Herrera, A. Nykjaer, B.L. Hempstead, and F.S. Lee. 2005. Sortilin controls intracellular sorting of brain-derived neurotrophic factor to the regulated secretory pathway. *J. Neurosci.* 25:6156–6166. http://dx.doi.org/10.1523/JNEUROSCI.1017-05.2005

Cheng, P.Y., A.L. Svingos, H. Wang, C.L. Clarke, S. Jenab, I.W. Beczkowska, C.E. Inturrisi, and V.M. Pickel. 1995. Ultrastructural immunolabeling shows prominent presynaptic vesicular localization of delta-opioid receptor within both enkephalin- and nonenkephalin-containing axon terminals in the superficial layers of the rat cervical spinal cord. *J. Neurosci.* 15:5976–5988.

Chiaruttini, C., A. Vicario, Z. Li, G. Baj, P. Braiuca, Y. Wu, F.S. Lee, L. Gardossi, J.M. Baraban, and E. Tongiorgi. 2009. Dendritic trafficking of BDNF mRNA is mediated by translin and blocked by the G196A (Val66Met) mutation. *Proc. Natl. Acad. Sci. USA*. 106:16481–16486. http://dx.doi.org/10.1073/pnas.0902833106

Conner, J.M., J.C. Lauterborn, Q. Yan, C.M. Gall, and S. Varon. 1997. Distribution of brain-derived neurotrophic factor (BDNF) protein and mRNA in the normal adult rat CNS: Evidence for anterograde axonal transport. *J. Neurosci.* 17:2295–2313.

Danzer, S.C., and J.O. McNamara. 2004. Localization of brain-derived neurotrophic factor to distinct terminals of mossy fiber axons implies regulation of both excitation and feedforward inhibition of CA3 pyramidal cells. *J. Neurosci.* 24:11346–11355. http://dx.doi.org/10.1523/JNEUROSCI.3846-04.2004

Dean, C., H. Liu, F.M. Dunning, P.Y. Chang, M.B. Jackson, and E.R. Chapman. 2009. Synaptotagmin-IV modulates synaptic function and long-term potentiation by regulating BDNF release. *Nat. Neurosci.* 12:767–776. http://dx.doi.org/10.1038/nn.2315

Diez, M., P. Schweinhardt, S. Petersson, F.H. Wang, C. Lavebratt, M. Schalling, T. Hökfelt, and C. Spenger. 2003. MRI and in situ hybridization reveal early disturbances in brain size and gene expression in the megencephalic (mceph/mceph) mouse. *Eur. J. Neurosci.* 18:3218–3230. http://dx.doi.org/10.1111/j.1460-9568.2003.02994.x

Dugich-Djordjevic, M.M., C. Peterson, F. Isono, F. Ohsawa, H.R. Widmer, T.L. Denton, G.L. Bennett, and F. Hefti. 1995. Immunohistochemical visualization of brain-derived neurotrophic factor in the rat brain. *Eur. J. Neurosci.* 7:1831–1839. http://dx.doi.org/10.1111/j.1460-9568.1995.tb00703.x

Egan, M.F., M. Kojima, J.H. Callicott, T.E. Goldberg, B.S. Kolachana, A. Bertolino, E. Zaitsev, B. Gold, D. Goldman, M. Dean, et al. 2003. The BDNF val66met polymorphism affects activity-dependent secretion of BDNF and human memory and hippocampal function. *Cell*. 112:257–269. http://dx.doi.org/10.1016/S0092-8674(03)00035-7

Ernfors, P., K.F. Lee, and R. Jaenisch. 1994. Mice lacking brain-derived neurotrophic factor develop with sensory deficits. *Nature*. 368:147–150. http://dx.doi.org/10.1038/368147a0

Fayard, B., S. Loeffler, J. Weis, E. Vögelin, and A. Krüttgen. 2005. The secreted brain-derived neurotrophic factor precursor pro-BDNF binds to TrkB and p75NTR but not to TrkA or TrkC. *J. Neurosci. Res.* 80:18–28. http://dx.doi.org/10.1002/jnr.20432

Frotscher, M., A. Drakew, and B. Heimrich. 2000. Role of afferent innervation and neuronal activity in dendritic development and spine maturation of fascia dentata granule cells. *Cereb. Cortex.* 10:946–951. http://dx.doi.org/10.1093/cercor/10.10.946

Galimberti, I., N. Gogolla, S. Alberi, A.F. Santos, D. Muller, and P. Caroni. 2006. Long-term rearrangements of hippocampal mossy fiber terminal connectivity in the adult regulated by experience. *Neuron*. 50:749–763. http://dx.doi.org/10.1016/j.neuron.2006.04.026

Galimberti, I., E. Bednarek, F. Donato, and P. Caroni. 2010. EphA4 signaling in juveniles establishes topographic specificity of structural plasticity in the hippocampus. *Neuron*. 65:627–642. http://dx.doi.org/10.1016/j.neuron.2010.02.016

Gall, C., L.M. Berry, and L.A. Hodgson. 1986. Cholecystokinin in the mouse hippocampus: Localization in the mossy fiber and dentate commissural systems. *Exp. Brain Res.* 62:431–437. http://dx.doi.org/10.1007/BF00238862

Goodman, L.J., J. Valverde, F. Lim, M.D. Geschwind, H.J. Federoff, A.I. Geller, and F. Hefti. 1996. Regulated release and polarized localization of brain-derived neurotrophic factor in hippocampal neurons. *Mol. Cell. Neurosci.* 7:222–238. http://dx.doi.org/10.1006/mcne.1996.0017

Gray, J., G.S. Yeo, J.J. Cox, J. Morton, A.L. Adlam, J.M. Keogh, J.A. Yanovski, A. El Gharbawy, J.C. Han, Y.C. Tung, et al. 2006. Hyperphagia, severe obesity, impaired cognitive function, and hyperactivity associated with functional loss of one copy of the brain-derived neurotrophic factor (BDNF) gene. *Diabetes*. 55:3366–3371. http://dx.doi.org/10.2337/db06-0550

Hartmann, M., R. Heumann, and V. Lessmann. 2001. Synaptic secretion of BDNF after high-frequency stimulation of glutamatergic synapses. *EMBO J.* 20:5887–5897. http://dx.doi.org/10.1093/emboj/20.21.5887

Haubensak, W., F. Narz, R. Heumann, and V. Lessmann. 1998. BDNF-GFP containing secretory granules are localized in the vicinity of synaptic junctions of cultured cortical neurons. *J. Cell Sci.* 111:1483–1493.

Heyden, A., M.C. Ionescu, S. Romorini, B. Kracht, V. Ghiglieri, P. Calabresi, C. Seidenbecher, F. Angenstein, and E.D. Gundelfinger. 2011. Hippocampal enlargement in Bassoon-mutant mice is associated with enhanced neurogenesis, reduced apoptosis, and abnormal BDNF levels. *Cell Tissue Res.* 346:11–26. http://dx.doi.org/10.1007/s00441-011-1233-3

Hofer, M., S.R. Pagliusi, A. Hohn, J. Leibrock, and Y.A. Barde. 1990. Regional distribution of brain-derived neurotrophic factor mRNA in the adult mouse brain. *EMBO J.* 9:2459–2464.

Isackson, P.J., M.M. Huntsman, K.D. Murray, and C.M. Gall. 1991. BDNF mRNA expression is increased in adult rat forebrain after limbic seizures: Temporal patterns of induction distinct from NGF. *Neuron*. 6:937–948. http://dx.doi.org/10.1016/0896-6273(91)90234-Q

Jakawich, S.K., H.B. Nasser, M.J. Strong, A.J. McCartney, A.S. Perez, N. Rakesh, C.J. Carruthers, and M.A. Sutton. 2010. Local presynaptic activity gates homeostatic changes in presynaptic function driven by dendritic BDNF synthesis. *Neuron*. 68:1143–1158. http://dx.doi.org/10.1016/j.neuron.2010.11.034

Jones, K.R., I. Fariñas, C. Backus, and L.F. Reichardt. 1994. Targeted disruption of the BDNF gene perturbs brain and sensory neuron development but not motor neuron development. *Cell*. 76:989–999. http://dx.doi.org/10.1016/0092-8674(94)90377-8

Karey, K.P., and D.A. Sirbasku. 1989. Glutaraldehyde fixation increases retention of low molecular weight proteins (growth factors) transferred to nylon membranes for western blot analysis. *Anal. Biochem.* 178:255–259. http://dx.doi.org/10.1016/0003-2697(89)90634-9

Kennedy, M.J., and M.D. Ehlers. 2011. Mechanisms and function of dendritic exocytosis. *Neuron*. 69:856–875. http://dx.doi.org/10.1016/j.neuron.2011.02.032

Kerr, A.M., and P. Jonas. 2008. The two sides of hippocampal mossy fiber plasticity. *Neuron*. 57:5–7. http://dx.doi.org/10.1016/j.neuron.2007.12.015

Kojima, M., N. Takei, T. Numakawa, Y. Ishikawa, S. Suzuki, T. Matsumoto, R. Katoh-Semba, H. Nawa, and H. Hatanaka. 2001. Biological characterization and optical imaging of brain-derived neurotrophic factor-green fluorescent protein suggest an activity-dependent local release of brain-derived neurotrophic factor in neurites of cultured hippocampal neurons. *J. Neurosci. Res.* 64:1–10. http://dx.doi.org/10.1002/jnr.1080

Kolbeck, R., I. Bartke, W. Eberle, and Y.A. Barde. 1999. Brain-derived neurotrophic factor levels in the nervous system of wild-type and neurotrophin gene mutant mice. *J. Neurochem.* 72:1930–1938. http://dx.doi.org/10.1046/j.1471-4159.1999.0721930.x

Korte, M., P. Carroll, E. Wolf, G. Brem, H. Thoenen, and T. Bonhoeffer. 1995. Hippocampal long-term potentiation is impaired in mice lacking brain-derived neurotrophic factor. *Proc. Natl. Acad. Sci. USA*. 92:8856–8860. http://dx.doi.org/10.1073/pnas.92.19.8856

Koshimizu, H., K. Kiyosue, T. Hara, S. Hazama, S. Suzuki, K. Uegaki, G. Nagappan, E. Zaitsev, T. Hirokawa, Y. Tatsu, et al. 2009. Multiple functions of precursor BDNF to CNS neurons: Negative regulation of neurite growth, spine formation and cell survival. *Mol. Brain*. 2:27. http://dx.doi .org/10.1186/1756-6606-2-27

Lang, S.B., V. Stein, T. Bonhoeffer, and C. Lohmann. 2007. Endogenous brain-derived neurotrophic factor triggers fast calcium transients at synapses in developing dendrites. *J. Neurosci*. 27:1097–1105. http://dx.doi.org/10 .1523/JNEUROSCI.3590-06.2007

Lavebratt, C., A. Trifunovski, A.S. Persson, F.H. Wang, T. Klason, I. Ohman, A. Josephsson, L. Olson, C. Spenger, and M. Schalling. 2006. Carbamazepine protects against megencephaly and abnormal expression of BDNF and Nogo signaling components in the mceph/mceph mouse. *Neurobiol. Dis*. 24:374–383. http://dx.doi.org/10.1016/j.nbd.2006.07.018

Leibrock, J., F. Lottspeich, A. Hohn, M. Hofer, B. Hengerer, P. Masiakowski, H. Thoenen, and Y.A. Barde. 1989. Molecular cloning and expression of brain-derived neurotrophic factor. *Nature*. 341:149–152. http://dx.doi .org/10.1038/341149a0

Li, Y., G. Calfa, T. Inoue, M.D. Amaral, and L. Pozzo-Miller. 2010. Activity-dependent release of endogenous BDNF from mossy fibers evokes a TRPC3 current and Ca2+ elevations in CA3 pyramidal neurons. *J. Neurophysiol*. 103:2846–2856. http://dx.doi.org/10.1152/jn.01140.2009

Link, W., U. Konietzko, G. Kauselmann, M. Krug, B. Schwanke, U. Frey, and D. Kuhl. 1995. Somatodendritic expression of an immediate early gene is regulated by synaptic activity. *Proc. Natl. Acad. Sci. USA*. 92:5734–5738. http://dx.doi.org/10.1073/pnas.92.12.5734

Louhivuori, V., A. Vicario, M. Uutela, T. Rantamäki, L.M. Louhivuori, E. Castrén, E. Tongiorgi, K.E. Akerman, and M.L. Castrén. 2011. BDNF and TrkB in neuronal differentiation of Fmr1-knockout mouse. *Neurobiol. Dis*. 41:469–480. http://dx.doi.org/10.1016/j.nbd.2010.10.018

Luo, X.G., R.A. Rush, and X.F. Zhou. 2001. Ultrastructural localization of brain-derived neurotrophic factor in rat primary sensory neurons. *Neurosci. Res*. 39:377–384. http://dx.doi.org/10.1016/S0168-0102(00)00238-8

Lyford, G.L., K. Yamagata, W.E. Kaufmann, C.A. Barnes, L.K. Sanders, N.G. Copeland, D.J. Gilbert, N.A. Jenkins, A.A. Lanahan, and P.F. Worley. 1995. Arc, a growth factor and activity-regulated gene, encodes a novel cytoskeleton-associated protein that is enriched in neuronal dendrites. *Neuron*. 14:433–445. http://dx.doi.org/10.1016/0896-6273(95)90299-6

Matsuda, N., H. Lu, Y. Fukata, J. Noritake, H. Gao, S. Mukherjee, T. Nemoto, M. Fukata, and M.M. Poo. 2009. Differential activity-dependent secretion of brain-derived neurotrophic factor from axon and dendrite. *J. Neurosci*. 29:14185–14198. http://dx.doi.org/10.1523/JNEUROSCI.1863-09.2009

Matsumoto, T., S. Rauskolb, M. Polack, J. Klose, R. Kolbeck, M. Korte, and Y.A. Barde. 2008. Biosynthesis and processing of endogenous BDNF: CNS neurons store and secrete BDNF, not pro-BDNF. *Nat. Neurosci*. 11:131–133. http://dx.doi.org/10.1038/nn2038

Mellman, I., and W.J. Nelson. 2008. Coordinated protein sorting, targeting and distribution in polarized cells. *Nat. Rev. Mol. Cell Biol*. 9:833–845. http:// dx.doi.org/10.1038/nrm2525

Miller, S., M. Yasuda, J.K. Coats, Y. Jones, M.E. Martone, and M. Mayford. 2002. Disruption of dendritic translation of CaMKIIalpha impairs stabilization of synaptic plasticity and memory consolidation. *Neuron*. 36:507–519. http://dx.doi.org/10.1016/S0896-6273(02)00978-9

Nicoll, R.A., and D. Schmitz. 2005. Synaptic plasticity at hippocampal mossy fibre synapses. *Nat. Rev. Neurosci*. 6:863–876. http://dx.doi.org/10.1038/ nrn1786

Nikoletopoulou, V., H. Lickert, J.M. Frade, C. Rencurel, P. Giallonardo, L. Zhang, M. Bibel, and Y.A. Barde. 2010. Neurotrophin receptors TrkA and TrkC cause neuronal death whereas TrkB does not. *Nature*. 467:59–63. http://dx.doi.org/10.1038/nature09336

Patterson, S.L., T. Abel, T.A. Deuel, K.C. Martin, J.C. Rose, and E.R. Kandel. 1996. Recombinant BDNF rescues deficits in basal synaptic transmission and hippocampal LTP in BDNF knockout mice. *Neuron*. 16:1137–1145. http://dx.doi.org/10.1016/S0896-6273(00)80140-3

Rattenholl, A., M. Ruoppolo, A. Flagiello, M. Monti, F. Vinci, G. Marino, H. Lilie, E. Schwarz, and R. Rudolph. 2001. Pro-sequence assisted folding and disulfide bond formation of human nerve growth factor. *J. Mol. Biol*. 305:523–533. http://dx.doi.org/10.1006/jmbi.2000.4295

Rauskolb, S., M. Zagrebelsky, A. Dreznjak, R. Deogracias, T. Matsumoto, S. Wiese, B. Erne, M. Sendtner, N. Schaeren-Wiemers, M. Korte, and Y.A. Barde. 2010. Global deprivation of brain-derived neurotrophic factor in the CNS reveals an area-specific requirement for dendritic growth. *J. Neurosci*. 30:1739–1749. http://dx.doi.org/10.1523/ JNEUROSCI.5100-09.2010

Rekart, J.L., C.J. Sandoval, F. Bermudez-Rattoni, and A. Routtenberg. 2007. Remodeling of hippocampal mossy fibers is selectively induced seven days after the acquisition of a spatial but not a cued reference memory task. *Learn. Mem*. 14:416–421. http://dx.doi.org/10.1101/lm.516507

Salio, C., S. Averill, J.V. Priestley, and A. Merighi. 2007. Costorage of BDNF and neuropeptides within individual dense-core vesicles in central and peripheral neurons. *Dev. Neurobiol*. 67:326–338. http://dx.doi.org/10 .1002/dneu.20358

Scharfman, H.E., A.L. Sollas, K.L. Smith, M.B. Jackson, and J.H. Goodman. 2002. Structural and functional asymmetry in the normal and epileptic rat dentate gyrus. *J. Comp. Neurol*. 454:424–439. http://dx.doi.org/ 10.1002/cne.10449

Schmidt-Kastner, R., C. Wetmore, and L. Olson. 1996. Comparative study of brain-derived neurotrophic factor messenger RNA and protein at the cellular level suggests multiple roles in hippocampus, striatum and cortex. *Neuroscience*. 74:161–183. http://dx.doi.org/10.1016/0306-4522(96)00093-0

Tanaka, J., Y. Horiike, M. Matsuzaki, T. Miyazaki, G.C. Ellis-Davies, and H. Kasai. 2008. Protein synthesis and neurotrophin-dependent structural plasticity of single dendritic spines. *Science*. 319:1683–1687. http://dx.doi .org/10.1126/science.1152864

Tao, X., S. Finkbeiner, D.B. Arnold, A.J. Shaywitz, and M.E. Greenberg. 1998. Ca2+ influx regulates BDNF transcription by a CREB family transcription factor-dependent mechanism. *Neuron*. 20:709–726. http://dx.doi.org/ 10.1016/S0896-6273(00)81010-7

Tongiorgi, E., M. Righi, and A. Cattaneo. 1997. Activity-dependent dendritic targeting of BDNF and TrkB mRNAs in hippocampal neurons. *J. Neurosci*. 17:9492–9505.

Tongiorgi, E., M. Armellin, P.G. Giulianini, G. Bregola, S. Zucchini, B. Paradiso, O. Steward, A. Cattaneo, and M. Simonato. 2004. Brain-derived neurotrophic factor mRNA and protein are targeted to discrete dendritic laminas by events that trigger epileptogenesis. *J. Neurosci*. 24:6842–6852. http://dx.doi.org/10.1523/JNEUROSCI.5471-03.2004

Vezzani, A., T. Ravizza, D. Moneta, M. Conti, A. Borroni, M. Rizzi, R. Samanin, and R. Maj. 1999. Brain-derived neurotrophic factor immuno-reactivity in the limbic system of rats after acute seizures and during spontaneous convulsions: Temporal evolution of changes as compared to neuropeptide Y. *Neuroscience*. 90:1445–1461. http://dx.doi.org/10 .1016/S0306-4522(98)00553-3

Wetmore, C., Y.H. Cao, R.F. Pettersson, and L. Olson. 1991. Brain-derived neurotrophic factor: Subcellular compartmentalization and interneuronal transfer as visualized with anti-peptide antibodies. *Proc. Natl. Acad. Sci. USA*. 88:9843–9847. http://dx.doi.org/10.1073/pnas.88.21.9843

Wu, Y.C., R. Williamson, Z. Li, A. Vicario, J. Xu, M. Kasai, Y. Chern, E. Tongiorgi, and J.M. Baraban. 2011. Dendritic trafficking of brain-derived neurotrophic factor mRNA: Regulation by translin-dependent and -independent mechanisms. *J. Neurochem*. 116:1112–1121. http:// dx.doi.org/10.1111/j.1471-4159.2010.07166.x

Wu, Y.J., A. Krüttgen, J.C. Möller, D. Shine, J.R. Chan, E.M. Shooter, and J.M. Cosgaya. 2004. Nerve growth factor, brain-derived neurotrophic factor, and neurotrophin-3 are sorted to dense-core vesicles and released via the regulated pathway in primary rat cortical neurons. *J. Neurosci. Res*. 75:825–834. http://dx.doi.org/10.1002/jnr.20048

Yan, Q., R.D. Rosenfeld, C.R. Matheson, N. Hawkins, O.T. Lopez, L. Bennett, and A.A. Welcher. 1997. Expression of brain-derived neurotrophic factor protein in the adult rat central nervous system. *Neuroscience*. 78:431–448. http://dx.doi.org/10.1016/S0306-4522(96)00613-6

Yang, J., C.J. Siao, G. Nagappan, T. Marinic, D. Jing, K. McGrath, Z.Y. Chen, W. Mark, L. Tessarollo, F.S. Lee, et al. 2009. Neuronal release of proBDNF. *Nat. Neurosci*. 12:113–115. http://dx.doi.org/10.1038/nn.2244

Zafra, F., B. Hengerer, J. Leibrock, H. Thoenen, and D. Lindholm. 1990. Activity dependent regulation of BDNF and NGF mRNAs in the rat hippocampus is mediated by non-NMDA glutamate receptors. *EMBO J*. 9:3545–3550.

Zakharenko, S.S., S.L. Patterson, I. Dragatsis, S.O. Zeitlin, S.A. Siegelbaum, E.R. Kandel, and A. Morozov. 2003. Presynaptic BDNF required for a presynaptic but not postsynaptic component of LTP at hippocampal CA1-CA3 synapses. *Neuron*. 39:975–990. http://dx.doi.org/10.1016/S0896-6273(03)00543-9

Zhao, S., D. Studer, X. Chai, W. Graber, N. Brose, S. Nestel, C. Young, E.P. Rodriguez, K. Saetzler, and M. Frotscher. 2012. Structural plasticity of hippocampal mossy fiber synapses as revealed by high-pressure freezing. *J. Comp. Neurol*. In press.

Zhou, X.F., X.Y. Song, J.H. Zhong, S. Barati, F.H. Zhou, and S.M. Johnson. 2004. Distribution and localization of pro-brain-derived neurotrophic factor-like immunoreactivity in the peripheral and central nervous system of the adult rat. *J. Neurochem*. 91:704–715. http://dx.doi.org/10.1111/ j.1471-4159.2004.02775.x

Zuccato, C., M. Valenza, and E. Cattaneo. 2010. Molecular mechanisms and potential therapeutical targets in Huntington's disease. *Physiol. Rev*. 90:905–981. http://dx.doi.org/10.1152/physrev.00041.2009